Mega parsec relativistic jets launched from an accreting supermassive blackhole in an extreme spiral galaxy

Joydeep Bagchi[1], Vivek M.[1], Vinu Vikram[2], Ananda Hota[3], Biju K.G.[4,7], S. K. Sirothia[5], Raghunathan Srianand[1], Gopal-Krishna[1,6], Joe Jacob[7]

ABSTRACT

Radio galaxy phenomenon is directly connected to mass accreting, spinning supermassive black holes found in the active galactic nuclei (AGN). It is still unclear how the collimated jets of relativistic plasma on hundreds to thousands of kpc scale form, and why nearly always they are launched from the nuclei of bulge dominated elliptical galaxies and not flat spirals. Here we present the discovery of giant radio source J2345-0449 ($z = 0.0755$), a clear and extremely rare counter example where relativistic jets are ejected from a luminous and massive spiral galaxy on scale of ~ 1.6 Mpc, the largest known so far. Extreme physical properties observed for this bulgeless spiral host, such as its high optical and infra-red luminosity, large dynamical mass, rapid disk rotation, and episodic jet activity are possibly the results of its unusual formation history, which has also assembled, via gas accretion from a disk, its central black hole of mass $> 2 \times 10^8$ $M_\odot$. The very high mid-IR luminosity of the galaxy suggests that it is actively forming stars and still building a massive disk. We argue that the launch of these powerful jets is facilitated by an advection dominated, magnetized accretion flow at low Eddington rate onto this unusually massive (for a bulgeless disk galaxy) and possibly fast-spinning central black hole. Therefore, J2345-0449 is an extremely rare, unusual galactic system whose properties challenge

[1]The Inter-University Centre for Astronomy and Astrophysics (IUCAA), Pune University Campus, Post Bag 4, Pune 411007, India; joydeep@iucaa.ernet.in

[2]Department of Physics and Astronomy, University of Pennsylvania, Philadelphia 19104, USA

[3]UM-DAE Centre for Excellence in Basic Sciences, Vidhyanagari, Mumbai 400098, India

[4]Department of Physics, W.M.O. Arts & Science College, Post Office Muttil, North Kalpetta, Wayanad, India

[5]National Centre for Radio Astrophysics (NCRA), TIFR, Pune University Campus, Post Bag 3, Ganeshkhind, Pune 411 007, India

[6]NASI Platinum Jubilee Senior Scientist

[7]Department of Physics, Newman College, Thodupuzha 685 585, India

the standard paradigms for black hole growth and formation of relativistic jets in disk galaxies. Thus, it provides fundamental insight into accretion disk – relativistic jet coupling processes.

Subject headings: galaxies: active – galaxies: jets – galaxies: individual (2MASX J23453268-0449256) – accretion, accretion disks – black hole physics

1. INTRODUCTION

It is now widely recognized that supermassive black holes (SMBH) of masses $\sim 10^6$-10^{10} $M_\odot$ lurk in the nuclei of almost all massive galaxies (e.g., Kormendy & Rishstone 1995; Magorrian et al. 1998). A symbiotic relationship between the growth of the central black holes and bulges of galaxies is suggested by a remarkably tight correlation between the masses of the black holes and the galactic bulges (Magorrian et al. 1998; Gebhardt et al. 2000; Haring & Rix 2004; Marconi & Hunt 2003). The most spectacular manifestations of massive black holes in AGN are the powerful bi-polar relativistic jets, that form twin-lobed giant radio galaxies on 10^2-10^3 kilo parsec (kpc) scale, and the extremely luminous quasars. Gravitational accretion of matter onto the SMBH is believed to be the 'central engine' that powers such sources (Lynden-Bell 1969; Soltan 1982) and their growth governed by accretion processes (Soltan 1982; Begelman et al. 1984). Understanding the physics of black hole formation and relativistic jets is a major focus of modern astrophysics. Powerful radio jets on $\gtrsim$100 kpc scale are nearly always launched from the nuclei of elliptical galaxies and not spirals, and the typical radio luminosity of spiral galaxies with AGN is about 10^3-10^4 times feebler than ellipticals, making them comparatively radio-quiet. Moreover, while both ellipticals and spirals may host radio-quiet quasars, radio-loud quasars are never found in spiral galaxies, but only in ellipticals, and about 10% of quasars are radio loud at a given epoch, for reasons that are still unknown (e.g., Dunlop et al. 2003).

The physical origin of radio-loud/radio-quiet dichotomy and mechanisms by which relativistic jets are launched from accretion disks around black holes (the disk-jet coupling) have long been the subject of intense investigations, yet the issue still remains unresolved despite a wealth of observations. It is plausible that the prime difference between radio-loud and radio-quiet AGN is connected to the fundamental black hole properties; namely its mass, spin and the accretion rate. Any theoretical model must explain why it is so difficult for massive black holes in disk galaxies to eject collimated radio jets extending to 10^2-10^3 kpc distances. The question whether the black hole mass or spin and radio loudness of AGN host are interconnected remains unanswered and is still under close scrutiny. It was suggested by Laor (Laor 2000) that only AGNs with black hole masses $\gtrsim 3\times$

10^8 $M_\odot$ in elliptical galaxies produce large scale jets, in contrast to smaller mass black holes found in spirals which obviously lack such jets. According to the 'spin-paradigm', powerful large scale jets originate near rapidly spinning accreting SMBHs (Wilson & Colbert 1995; Sikora et al. 2007; Tchekhovskoy et al. 2010; Dotti et al. 2013) found in bulge dominated systems, and launched at relativistic speeds via the magneto-hydrodynamic (MHD) Blandford-Znajek (BZ) mechanism (Blandford & Znajek 1977; MacDonald & Thorne 1982; Penna et al. 2013), although observational evidence for this conjecture is sparse (Wang et al. 2006; Doeleman et al. 2012). Alternatively, in the Blandford-Payne (BP) mechanism (Blandford & Payne 1982), jet power is extracted from the rotation of the accretion disk itself, via the magnetic field threading it, without invoking a rapidly spinning black hole. However, in both the processes the intensity and geometry of the magnetic field near the black hole horizon strongly influences the Poynting flux of the emergent jet (Beckwith & Hawley 2008). This has given rise to the 'magnetic flux paradigm' which posits (Sikora & Begelman 2013) that jet launching and collimation requires strong magnetic flux anchored to an ion-supported torus of optically thin, geometrically thick, extremely hot gas having poor radiative efficiency (Rees et al. 1982). Such hot, magnetic field saturated ion-tori may arise naturally around spinning black holes via advection dominated accretion flows (ADAF) at low Eddington rates (Eddington luminosity for a black hole of mass M is; $L_{Edd} = 1.26 \times 10^{38} M/M_\odot$ erg s^{-1}), particularly in elliptical galaxies showing large scale jets (Narayan & Yi 1994; Narayan & Yi 1995). On the other hand, for AGN in spirals (narrow-line Seyfert 1s, optically selected quasars), the mass accretion rates are plausibly near Eddington, forming optically thick, geometrically thin accretion disks which radiate efficiently, but fail to create large-scale collimated radio jets.

The physical mechanism linking the super massive black hole mass to the galactic bulge properties is little understood, while it is believed that an energetic AGN feedback, either via the mechanical power of the radio jets, or through a pressure driven wind, on the surrounding medium, plays a major role in regulating the growth of the black hole and even the surrounding host galaxy. Important details of how SMBH grow, and their energetic feedback processes are still missing, but it is gradually becoming clear that SMBH are essential ingredients shaping the lives of galaxies across the cosmic time (for review see Alexander & Hickox 2012). Thus a detailed study of active galaxies hosting massive black holes assumes great importance; particularly finding any clear counter examples of jet launching under extremely unusual circumstances, such as the case of radio galaxy J2345-0449 presented in this work, may play a key role in informing us what factors determine the relativistic jet formation and its role in galaxy evolution.

Our paper is organized as follows; In Sec. 2 we introduce the radio source J2345-0449 and highlight its main radio and optical properties. In Sec. 3 we present the radio, optical and mid-IR observations of the source, describe the data analysis procedure in detail and obtain

the main results. In Sec. 4 we focus on the scientific content of the results and discuss their wider astrophysical implications. Finally, in Sec. 5 we present our main discussion and conclusions in light of the results obtained above, and highlight the possibilities of future multi wavelength observations for an in-depth understanding of this extraordinary galaxy.

We adopt a ΛCDM cosmology model with $H_0 = 70.5$ km s^{-1} Mpc^{-1}, $\Omega_M = 0.27$ and $\Omega_\Lambda = 0.73$, which results in a scale of 1.43 kpc arcsec^{-1} for a redshift $z = 0.0755$. The radio spectral index α is defined as: flux density $(S_\nu) \propto$ frequency $(\nu)^{-\alpha}$.

2. A JET-LAUNCHING MASSIVE SPIRAL GALAXY 2MASX J23453268-0449256

Our most important finding is the extraordinary galaxy 2MASX J23453268-0449256 at a redshift $z = 0.0755$ (hereafter called J2345-0449), which is an extremely rare and clear example of megaparsec (Mpc) scale collimated pair of relativistic plasma jets launched from the nucleus of a massive spiral galaxy. This radio galaxy was first mentioned by Machalski et al. (2007) as a Mpc-scale object located at redshift $z = 0.0757$, but they did not provide any further hints about its extraordinary nature. Our *Very Large Array* (VLA) and *Giant Meterwave Radio Telescope* (GMRT)[1] images in Figure 1 show that the synchrotron radio emission arises from an enormous (>Mpc scale) bipolar structure with two pairs of radio lobes, i.e. forming a giant 'double-double' radio galaxy (DDRG) centered on the spiral host. With two nearly aligned pairs of radio lobes sharing a common AGN core, DDRGs are the most compelling, rare examples of recurring jet activity of SMBHs (Schoenmakers 2000; Saikia & Jamrozy 2009). Remarkably, the inner and outer radio lobe pairs extend over $\sim$ 387.2 kpc ($\sim 4.52'$) and $\sim$ 1.63 Mpc ($\sim 19.1'$), respectively, making J2345-0449 the largest radio source known till date, hosted by a spiral galaxy. The VLA 6cm (4.8 GHz) image shows that inner 'active' radio lobes are of edge-brightened (Fanaroff-Riley class II or FRII (Fanaroff & Riley 1974)) morphology, being fed by the collimated jets shot out from the central nucleus, which is typical of DDRGs (Schoenmakers 2000; Saikia & Jamrozy 2009). The GMRT low frequency 330 MHz image shows that the 'aged' outer lobes are more diffuse, lacking prominent hot spots, no longer being energized by jets. The diffuse steep-spectrum radio emission near inner lobes is better visible in the lower frequency image, tracing the back flowing plasma of outer lobes. The integrated flux density and radio luminosity at 1.4 GHz are $S_{1.4} = 180.60 \pm 20.0$ mJy and $L_{1.4} = 2.5(\pm 0.3) \times 10^{31}$ erg s^{-1} Hz^{-1} respectively. Although moderate, this luminosity is much above the rough divide between the radio-quiet

[1] http://gmrt.ncra.tifr.res.in/

and radio-loud galaxies which is usually taken at $L_{1.4} \sim 10^{30}$ erg s^{-1} Hz^{-1}. However, despite a clear FRII morphology on large scales, the 1.4 GHz radio luminosity of J2345-0449 is close to the luminosity break between the FRI and FRII radio galaxies. The integrated flux density and radio luminosity at 330 MHz are $S_{330} = 3.60 \pm 0.15$ Jy and $L_{330} = 5.0(\pm 0.2) \times 10^{32}$ erg s^{-1} Hz^{-1} respectively, implying a very steep spectral index $\alpha_{330}^{1.4} \approx 2$ between 1.4 GHz and 330 MHz. Both the outer lobes have a very steep integrated radio spectral index $\alpha_{330}^{1.4} \sim 2$. We observe a sharp increase in $\alpha_{330}^{1.4}$ between the inner and outer lobes on both sides of the flat spectrum core, as expected due to radiative ageing of radio plasma in the episodic jet activity scenario (Figure 2).

The galaxy's favorable inclination the line-of-sight ($i \simeq 59°$) has enabled a direct view of the well-developed, bright spiral arms, as seen from the deep, high resolution optical images taken with the *MegaCam* camera on the Canada-France-Hawaii Telescope (CFHT) and also visible in the *Sloan Digital Sky Survey* (SDSS) multi-band images (Ahn et al. 2014) shown in Figures 3 and 6. The *Fermi* Gamma-ray telescope observations have recently indicated the presence of relativistic jets in a handful of spiral galaxies hosting narrow-line Seyfert 1 (NLSy1) nuclei (Abdo et al. 2009). While those jets are also very rare, they are not known to extend much beyond the galactic scale ($\lesssim$ 10 kpc) and lack the excellent collimation witnessed in the large-scale FRII jets (Doi 2012; Morganti 2011). It has been pointed out (Foschini 2011) that the Blandford-Znajek mechanism fails to explain the jet power of these jets. Thus, the nature of radio emission in NLSy1s and their failure to produce large-scale radio jets has remained unexplained. Despite decades of extensive observations, only two previous reports exist of a disk galaxy ejecting large scale (>100 kpc) bipolar radio jets: the radio source J031552-190644 found in the galaxy cluster Abell 428 (Ledlow et al. 1998), and a recently reported Mpc-scale episodic radio source known as *Speca* (Hota et al. 2011). In both these exceptionally rare objects, the galactic disk is viewed nearly edge-on, precluding a clear view of the putative spiral arms, and thus the evidence is still indirect. The present giant radio source J2345-0449 is not only the most unambiguous example of this extremely rare class, but its spiral host galaxy also displays a unique combination of several other remarkable properties (as discussed below). Extremely unusual objects like J2345-0449 strongly challenge the conventional ideas of black hole growth and radio jet formation in galactic nuclei, thus, they are of profound interest for models of the central engines of radio galaxies and quasars.

We used SDSS-III images (Ahn et al. 2014) to explore the large scale galactic environment in which the spiral galaxy J2345-0449 is located. The SDSS wide-field color image in Figure 3 and mid-IR data (Table 3) reveals that J2345-0449 is an unusually bright ($m_r = 14.40$, $M_r = -23.26$ in r band, $m_{12} = 9.00$, $M_{12} = -28.66$ in 12μm band) isolated spiral galaxy located in a sparsely populated galactic environment devoid of bright L* galaxies,

and clearly not at the center of a compact group or a rich galaxy cluster. The next brightest galaxy neighbour, which is located ∼460 kpc to the south east, is more than two magnitudes fainter. The second and third brightest galactic neighbours are $\gtrsim$2.5 magnitudes fainter and located ∼240 and 480 kpc away respectively (Figure 3). Interestingly, about 33 arcmin (∼2.8 Mpc) away from J2345-0449 (redshift $z = 0.07556$) is located a massive galaxy cluster RBS 2042 (redshift $z = 0.07860$) which is strongly detected in the ROSAT All-sky Bright Survey (Voges et al. 1999; Schwope et al. 2000). Association of J2345-0449 with this cluster is not immediately obvious, but it could be a peripheral member of the massive cluster.

3. OBSERVATIONS AND DATA ANALYSIS

3.1. GMRT observations

The 325 MHz data were obtained from the archives of GMRT. The observations were taken on 2008 November 25, with the total on source integration time of 5.8 hrs. The observations were taken at the frequency 325 MHz with a 32 MHz band-width. The primary flux density calibrator was 3C48 having flux density of 43.425 Jy at 325 MHz on the VLA (1999) Perley-Taylor scale. The phase calibrator was J2340+135 having a flux density 7.74 Jy at 325 MHz. The data reduction was done mainly using `AIPS++`[2]. After applying bandpass corrections on the phase calibrator, gain and phase variations were estimated, and the flux density, bandpass, gain and phase calibration parameters from primary and phase calibrator were applied on the target field. Bad quality data were flagged at various stages. The data for antennas with high errors in the antenna-based solutions were examined and flagged over certain time ranges. Some baselines were flagged based on closure errors on the bandpass calibrator. Channel and time-based flagging of data points corrupted by radio frequency interference (RFI) was done using a median filter with a 6σ threshold. Residual errors above 5σ were also flagged after a few rounds of imaging and self-calibration. The system temperature (T_{sys}) was found to vary with antenna, the ambient temperature and elevation. In the absence of regular T_{sys} measurements for GMRT antennas, this correction was estimated from the residuals of corrected data with respect to the model data. The corrections were then applied to the data. The final image was made after several rounds of phase self calibration, and one round of amplitude self-calibration, where the data were normalized by the median gain for all the data. On cleaned map (Figure 1) with FWHM beam $15.22'' \times 11.35''$ at a position angle of 62.3°, the root-mean-square noise level near the source is 1.1 mJy/beam. On highest resolution map (not shown) of FWHM beam $10.08'' \times 7.53''$,

[2] `http://aips2.nrao.edu/docs/aips++.html`

the rms noise level was 0.23 mJy/beam.

3.2. VLA observations

Very Large Array (VLA) C-band (6cm wavelength) data for J2345-0449 was obtained from the VLA archives. The observations were taken on 2008 June 27, in D-configuration, at the 4.88 GHz and 4.83 GHz centre frequencies, and using two IF pairs of 50 MHz band-width each. The primary flux density calibrator was 3C48 having flux density of 5.517 Jy and 5.570 Jy for the two IFs on the VLA (2010) flux density scale. The total integration time at the radio galaxy's core position was about 40 minutes and VLA calibrator source J2358-103 was periodically observed for phase calibration. For data reduction we used standard routines available in the *Astronomical Image Processing System* (AIPS) software. While calibrating, bad quality data were flagged at various stages. After initial amplitude and phase calibration the data of two IFs were combined. Further data editing and final imaging using a visibility weighting scheme (ROBUST = 2.5) in the imaging+deconvolution program IMAGR resulted in good quality radio maps (Figure 1). After deconvolution, the final clean map was restored with an elliptical Gaussian beam of FWHM $19.8'' \times 13.3''$ at position angle 178.5°. The root-mean-square noise on the clean map, measured near the centre was about 20μJy/beam. The compact AGN core was strongly detected with flux density 4.23 ± 0.10 mJy, and peak located at (positional error ± 0.15 arcsec) right ascension: $23h\ 45m\ 32.71s$ and declination: $-04^\circ\ 49'\ 25.18''$. The AGN radio core coincides within errors with the optical nucleus of the spiral galaxy, measured on the CFHT image at right ascension: $23h\ 45m\ 32.71s$ and declination: $-04^\circ\ 49'\ 25.32''$. The positional coincidence firmly establish the spiral as the optical host of this giant radio galaxy (Figure 1).

3.3. Evidence for interruption of the AGN jet activity

Figure 2 shows the spectral index map and a 1D spectral index profile computed between GMRT 325 MHz and NVSS 1400 MHz, after smoothing the 325 MHz map to the resolution of the latter, i.e. $45'' \times 45''$ beam. In the spectral index map all pixels having flux density below 2 mJy/beam at 1400 MHz ($\sim 4\sigma$) and 15 mJy/beam at 325 MHz ($\sim 5\sigma$) have been blanked to prevent spurious structures from appearing in the map. The 1D profile is drawn along the ridge line of the source defined by the brightness peaks seen on the full resolution 325 MHz GMRT map (Figure 1). The most conspicuous aspect of the profile is the sharp increase in spectral index seen immediately beyond the brightness peaks identified here as the inner double. The inner 'active' lobes have relatively flatter spectra and are fed by the

radio jets, showing edge-brightened FRII morphology, consistent with their interpretation as recently formed sources still being energized by the jets. This behaviour is fully consistent with the canonical interpretation of such double-double radio sources where the outer double lobes are viewed as the 'relics' of a previous episode of nuclear activity (Schoenmakers 2000; Saikia & Jamrozy 2009).

3.4. Optical Spectroscopic Observations and Data Analysis

Optical long-slit spectroscopic data were taken during 2011 November 20-22 with the 2m telescope at the IUCAA Girawali Observatory (IGO). The spectra were obtained using the IUCAA Faint Object Spectrograph and Camera (IFOSC) [3]. IFOSC employs an EEV 2K×2K, thinned, back-illuminated CCD with 13.5μm pixels. The spatial sampling scale at the detector is 44μm per arcsecond giving a field of view of about 10.5 arcminute on the side. We used two IFOSC grisms; grism No.7 and grism No.8 in combination with a 1.5-arcsec slit, yielding a wavelength coverage of 3800-6840 Å and 5800-8350 Å and spectral resolutions of 300 km/s and 240 km/s respectively. The spectra were taken with the slits aligned both along the major and minor axes of the galaxy. In each case, we took 4 exposures (4× 45 min) using the grism No.8 and 2 exposures (2× 45 min) using grism No.7, respectively. We carried out the bias and flat-field corrections to all the frames. Dark correction was not required as the CCD was liquid nitrogen cooled and the dark current was negligible for 45 min exposures. The cosmic ray hits were removed by the IRAF task 'crmedian' in the Cosmic Ray Removal Utility Package (CRUTIL). Standard stars were observed during the same nights by placing them at different slit locations. Wavelength calibration was done using the standard Helium-Neon lamp spectra.

One dimensional spectra were extracted using the *doslit* task in the IRAF software. We used the variance-weighted extraction method as compared to the normal one. Air-to-vacuum conversion was applied before combining the spectra using $1/\sigma^2$ weighting in each pixel after scaling the overall individual spectrum to a common flux level within a sliding window. The extraction was carried out both with and without cosmic ray removal. Fringing poses a problem for the grism No.8 (red region) data and we removed the fringes by subtracting two 2D science exposures for which the object was placed at two different locations along the slit. From the absorption and emission features in the spectrum (shown in Fig. 4), redshift of the galaxy was determined to be $z = 0.0755 \pm 0.0005$. We compared our spectrum with the 6dF spectrum given by Jones et al. (2009). The features in both the

[3] `http://www.iucaa.in/resources.html`

spectra match closely and our redshift estimate is very close to the reported 6dF redshift $z = 0.075566 \pm 0.000150$.

As the galaxy is spatially well resolved, we also performed the 2D spectral extraction around the Hα line detected in the grism No.8 spectra. For spectral curvature corrections, the spectra of a standard star (Feige 110) were taken at different spatial positions along the slit during the scheduled nights and nearby nights. The same standard star was used for the flux calibration. We created a superimposed frame by joining the different standard star spectra to the target spectra, retaining the original spatial position of each spectra. The data were then corrected for the geometrical distortions using the IRAF tasks *fitcoords* and *transform*. *Fitcoords* provides the transformation of slit position and wavelength as a function of (x,y) pixel number on the image. *Transform* applies this transformations to the data to correct the distortions. The resulting frame is used for the spectral extraction.

3.5. Deriving the Galaxy Rotation Curve

We carried out the curvature correction (as above) for each of the four exposures and then added them after proper shifting to improve the signal-to-noise ratio. We made sure that the addition is proper by looking at the residuals in the difference of the frames. We extracted 1D spectra from sub-apertures of 5 pixel width (spatial direction) placed symmetrically around the center of the galaxy. This has resulted in 15 individual spectra. The width of sub-aperture corresponds to an angular scale of ~ 1.5 arc sec (2.1 kpc), commensurate with typical seeing during the observing nights. In Figure 5 we show 2D spectrum image around the Hα and [N II] emission lines with the above sub-apertures marked. In the spectrum both the Hα and [N II] lines clearly show the signatures of a rapidly rising and then flat rotation curve.

We simultaneously fitted the Hα λ6562.81 $\mathring{A}$ and [N II] λ6585.27 $\mathring{A}$ lines using Gaussians and χ^2 minimization. The second [N II] $\lambda\,6549.86\,\mathring{A}$ line to the blue side of Hα line was faint, well within the noise, and thus we did not attempt to fit it. The rotational velocity V at each sub-aperture position was computed using the equation,

$$V = \frac{z_{\rm ap} - z_{\rm cen}}{(1 + z_{\rm cen})}\ 3 \times 10^5\ \ {\rm km\,s^{-1}} \qquad (1)$$

and plotted against the distance from nucleus to obtain the rotation curve. Here z_{ap} is the fitted redshift of the Hα line in a given aperture, and $z_{cen} = 0.0755$, the redshift at the dynamical center of the galaxy. The 2D extraction is carried out for the minor axis in the same manner as for the major axis data.

In Figure 6, we show the derived rotation curves for the major (red data points) and minor (blue data points) axis data. The major axis data shows a clear rotation signature while no disk rotation is evident along the minor axis. This is a clear evidence that the emission lines originate in a tilted, rotating disk. The rotational curve shown in Figure 5 is fitted with an analytical function (Courteau 1997)

$$V(R) = V_0 + \frac{2}{\pi} V_{\rm c,obs} \times \arctan^{-1}\left(\frac{R}{R_{\rm turn}}\right) \tag{2}$$

where, R is radial distance, V_0 is the systemic velocity, $V_{\rm c,obs}$ is the asymptotic circular velocity and $R_{\rm turn}$ is the turnover radius. The χ^2 minimised fitting led to the following values: $\rm V_0$ = 0 km s^{-1}, $\rm V_{c,obs}$ = 370.8±25.8 km s^{-1} and $\rm R_{turn}$=1.4±0.7 kpc. Finally, The inclination corrected circular velocity is derived at $\rm V_{c,incl}$ = 429.3±25.8 km s^{-1}. We have derived the inclination angle ($i = 59.7^\circ \pm 2^\circ$) using Hubble's standard formula

$$sin(i) = \left[\frac{(1-q^2)}{(1-q_0^2)}\right]^{1/2} \tag{3}$$

where $q = (a/b)$ is the apparent axial ratio of the galaxy, as obtained from the fitted r-band semi-minor and semi-major isophotal diameters of the disk (Table 2), and q_0 is the intrinsic axial ratio, i.e. the ratio of vertical to horizontal scale-heights of the disk. We have adopted a standard value $q_0 = 0.19$, although it varies slightly from disk to disk.

3.6. The Central Velocity Dispersion

The velocity dispersion measurements were performed using the *pPXF* (penalised PiXel Fitting) method (Cappellari & Emsellem 2004). The *pPXF* method extracts the line of sight velocity distributions of the stars from the observed galaxy spectra, parametrized using a Gauss-Hermite series. The code uses a penalty function that is derived from the integrated square deviation of the line profile from the best-fitting Gaussian. The fit is iterated until the penalty function cannot decrease the variance of the fit any further. The algorithm finds the mean velocity V and velocity dispersion σ which minimizes the difference between the observed galaxy spectrum and the spectrum of a stellar template convolved by the corresponding Gaussian. We used the single-age, single-metallicity, stellar population library of (Vazdekis 1999) as the template. Best-fit values of σ from fitting the $\rm Mg_b$ (λ 5175 Å) line, after correcting for the redshift and instrumental broadening, are $\sigma_* = 379(\pm25)$ km s^{-1} with the slit oriented along the major axis, and $\sigma_* = 351(\pm25)$ km s^{-1} along the minor axis. Both values are spatially averaged over 5 pixels (2.35 kpc) centered on the galactic nucleus.

3.7. Central AGN, Star Formation Rate and Metallicity

To decouple the possible AGN lines from the galaxy spectrum, we extracted the nuclear spectrum of only the central 5 pixels. In the nuclear spectra, a narrow [N II] line (λ 6583 Å) of FWHM $\sim$ 400 km/s is detected, while the Hα λ 6563 Å line is very weak and not reliably detected. Apart from these features we find no other definitive signature of AGN in the optical spectrum. The luminosities are: $3.02 \pm 0.27 \times 10^{40}$ erg s^{-1} for the [N II] and $< 1.05 \times 10^{40}$ erg s^{-1} (3σ) for Hα line. The [N II]/Hα line ratio lies above that for HII regions in the BPT diagnostic diagram (1) and it is a distinct signature of ongoing AGN activity. The small Hα luminosity shows that this AGN is a low-luminosity active galactic nucleus (LLAGN/LINER type), which are defined by having an Hα luminosity smaller than 10^{40} erg s^{-1} and weak emission lines, further indicating a very small mass accretion rate compared to the Eddington rate (equation 10).

For the disk extended emission, from the fitting of 2D spectra, we computed the integrated flux in the Hα and [N II] lines at different locations of the galaxy along the major and minor axes. The Hα fluxes were used to determine the star formation rates (SFR) and the Hα to [N II] flux ratios were used for calculating the metallicities. For estimating the SFR we used the equation

$$log(\mathrm{SFR}) = \epsilon_{H\alpha} log L(H\alpha) - log(\eta_{H\alpha}) \tag{4}$$

where, $\epsilon_{H\alpha}$ and $\eta_{H\alpha}$ values were taken from (Argence & Lamareille 2009) where dust correction is assumed to be negligible. The surface star formation rates are obtained by dividing the calculated SFR values by the area over which the extraction is done. For metallicity, we have used the formula (Pettini & Pagel 2004),

$$12 + log(\mathrm{O/H}) = 8.9 + 0.57 \times \log([\mathrm{NII}]/\mathrm{H}\alpha) \tag{5}$$

where O/H is the ratio of Oxygen to Hydrogen abundance, a proxy for metallicity. The variation of SFR and metallicity along the radial direction from centre is shown in Figure 7. While the surface SFR remains virtually constant, a radial gradient in metallicity across the disk is clearly evident. This indicates J2345-0449 is a spiral galaxy having a large SFR. Also notable is a striking lack of recent star formation activity near the galactic center, that is possibly attributed to energetic feedback from the central AGN, as discussed below.

3.8. *WISE* mid-infrared (MIR) colors

The spiral galaxy J2345-0449 is strongly detected in the mid-IR bands centered at 3.4, 4.6, 12 and 22 μm (W1, W2, W3 and W4 bands), observed by the *Wide-field Infrared Survey*

Explorer (WISE) satellite (Wright et al. 2010). The S/N ranges from 47.9 in 3.4 μm band to 10.9 in 22 μm band. The MIR magnitudes, luminosities and their errors are listed in Table 3. The very high MIR luminosity of the galaxy is unusual and suggests that it is actively forming stars and still building a massive stellar disk. We use the MIR colors to obtain the properties of a possibly dust obscured galactic nucleus and determine the radiative efficiency of the AGN. MIR data are highly suitable for this purpose because the optical-UV radiation from the AGN accretion disk is absorbed by the putative dusty-torus and re-radiated in MIR bands. It has been shown that WISE MIR colors can effectively distinguish AGN from star forming and passive galaxies and, moreover, within the AGN subset itself high-excitation radio galaxies (HERG) and low-excitation radio galaxies (LERG) stand out on the MIR color-color and MIR-radio plots (Stern et al. 2012; Gurkan et al. 2014). The MIR colors for J2345-0449 are:

$$[W1 - W2] = 0.064,\ [W2 - W3] = 2.817,\ [W2 - W4] = 4.722 \tag{6}$$

From the blue [W1 - W2]$<<$ 0.6 and red [W2 - W3]$\sim$3 colors we conclude that J2345-0449 is a star-forming spiral galaxy and there is negligible re-radiated MIR flux (no MIR 'bump') from the accretion disk (Wright et al. 2010; Stern et al. 2012). This is further corroborated by the position of J2345-0449 on the [W3]-L_{151} and [W4]-L_{151} planes. Here L_{151} is 151 MHz radio luminosity, which is estimated from the radio spectrum and using the spectral index value $\alpha = 2$ as calculated in Sec. 2. On these planes HERGs can be clearly distinguished from LERGs (Gurkan et al. 2014) and J2345-0449 is located in the region of LERGs (plot not shown here). Clearly, J2345-0449 is a low-excitation radio galaxy hosted by a spiral galaxy, presently its black hole is possibly residing in a low radiative efficiency (ADAF) state, as also indicated by the weak Hα and the lack of broad emission lines in the optical nuclear spectrum (Figure 4).

3.9. CFHT Imaging and Photometric Analysis: Bulge-Disk Decomposition

Modelling the light distribution in terms of bulge and the disk components of the spiral galaxy J2345-0449 is important for understanding the formation and evolution of this highly unusual galaxy and its central black hole. For this purpose we used the excellent quality archival data taken with the *MegaCam* wide-field imaging camera on the 3.6 meter Canada-France-Hawaii Telescope (Boulade et al. 2013). These images were processed, stacked and calibrated using the *MegaPipe* pipeline (Gwyn 2008) at the Canadian Astronomical Data Centre. We used the g and r band images taken in excellent seeing conditions of 0.75 and 0.80 arcsec (FWMH) and having effective exposure times of 960 and 1320 seconds respectively.

The *g*-band image was generated by stacking eight images taken during 2008 September 01 to 2009 December 13. Eleven images taken during the same period are used to obtain stacked *r*-band image. The individual images were median stacked using *SWarp* program (Bertin et al. 2002). The pixel scale of the stacked images was 0.18 arcsec. The *MegaPipe* also provided the inverse variance weight map for the stacked images. For additional tests and consistency check we also used the *g, r, i* and *z* band images from the SDSS.

For obtaining the bulge and disk parameters we used *PYMORPH* toolbox (Vikram et al. 2010) which has a Python based pipeline for two dimensional bulge-disk decomposition. *PyMorph* uses SEXTRACTOR (Bertin & Arnouts 1996) and GALFIT (Peng et al. 2002) for object detection and decomposition. Briefly, we created a cutout of the galaxy based on the half light radius of the object. The cutout size is selected wide enough to include enough sky pixels to model the sky background accurately. This size is set to ten times the half light radius for the current case. We found that the fitting results do not change significantly with the cutout size. After making the cutout image we generated a mask image which masks all the bad pixels and neighbouring objects during the fitting. The galaxy under study does not have any close neighbours (Figure 3), and therefore the contamination from neighbours is minimal. Next, we created a configuration file for GALFIT. The configuration file includes optimal initial values for the parameters of both bulge and disk. We derived the initial values using SEXTRACTOR parameters. We set the total bulge and disk magnitude to the MAG_AUTO parameter and the radius to the half light radius of the galaxy. The ellipticity and position angle are derived from the ELONGATION and THETA_IMAGE. A detailed description of the procedure can be found in (Vikram et al. 2010).

We used a composite of the Sérsic and an exponential function to model the galaxy light profile, where the former models the bulge and the latter models the disk. The form of the Sérsic function is

$$\Sigma(r) = \Sigma_e \exp\left(-\kappa\left[(r/r_e)^{1/n} - 1\right]\right) \tag{7}$$

where κ is a function of Sérsic index (n). For $n = 4$, $\kappa = 7.67$ which corresponds to the de Vaucouleurs law. Σ_e is the surface brightness at r_e, the scale radius (half light radius). The disk component is modeled using the exponential law which is given by

$$\Sigma(r) = \Sigma_0 e^{-(r/r_d)} \tag{8}$$

where Σ_0 is the central surface brightness and r_d is the disk scale length. The half light radius (r_e) is related to disk scale length as $r_e = 1.68 \times r_d$ and $\Sigma_e = \Sigma_0/5.36$.

The bulge-disk decomposition was done by χ^2 minimization. In this technique the observed image is compared to a PSF convolved linear combination of Sérsic and exponential

functions. Therefore, it was necessary to model the point spread function (PSF) well in order to reliably estimate the photometric parameters. We used stellar images closer to the galaxy to represent the PSF. For that we selected stars from the CFHT images based on the CLASS_STAR parameter from SEXTRACTOR and create stamp size images. These stellar images were checked manually using the IMEXAMINE program in IRAF. This helped to remove saturated stars and some other stars which are contaminated by bright neighbours. In Table 1 and Table 2 we list the fitted values of the bulge and disk parameters estimated using the g and r band CFHT images and the SDSS images. We found CFHT results fairly consistent with those obtained using the SDSS images, although the former were obtained under better seeing conditions. Although we used the pipeline, we vary the initial conditions of different parameters to check whether the final results correspond to a global minimum. We found that the results are stable against different initial conditions. Finally, we checked for any possible contribution from a possible point source at the center of the galaxy. We found that any such point source must be too faint and its inclusion doesn't improved the fit. The magnitudes shown in Table 1 and Table 2 have been corrected for foreground extinction using Schlegel et al. (Schlegel et al. 1998). We also applied k-correction using E/S0 SED from Poggianti et al. (Poggianti 1997). Figure 8 shows a comparison of the modelled profiles of bulge and disk components with the observed profile of the galaxy in the CFHT g and r bands. These are generated using IRAF/ELLIPSE task from the PSF convolved output images generated by GALFIT. It can be seen that the bulge-disk model agrees very well with the observed profile of the galaxy.

The Sérsic index for the bulge is found to be small at $n \approx 1$, which essentially implies a 'pseudo-bulge' with a disk-like exponential light profile ($n = 1$ gives a pure exponential profile, and $n = 4$ corresponds to the de Vaucouleurs profile). Moreover, the scale length of the bulge is very small compared to the disk ($r_d \approx 7 \times r_e$) and only about $14 - 18\%$ fraction of the total g-band or r-band luminosity is contributed by the bulge. This again indicates that the J2345-0449 spiral host contains a pseudo-bulge rather than a classical bulge component. Galaxies with classical bulges generally have a much more centrally peaked light profile, contain a higher fraction of total light and their Sérsic index is larger ($n \approx 2 - 6$), as compared to pseudo-bulges which have $n < 2$ (Fisher & Drory 2008; Kormendy et al. 2010).

3.10. Additional checks to confirm the pseudo-bulge nature of J2345-0449

We have compared several photometric parameters of the (pseudo) bulge in J2345-0449 to some other well known previous studies in order to further verify its pseudo bulge classification. According to (Gadotti 2009), pseudo bulges have small Sérsic index and scale

radius and they occur in galaxies having low bulge to total light ratio (B/T). Our estimated values of these parameters (Table 1 and 2) fall very close to those of pseudo bulge systems in (Gadotti 2009). We further compared our values with those of galaxies studied by (Fisher & Drory 2008). In Figure 9 we show that our fitted values for J2345-0449 fall near the pseudo bulge galaxies in $n_b - M_V$, $n_b - \mu_e$ and $n_b - r_e$ planes of (Fisher & Drory 2008). Similar trends were found in the $\mu_e - M_V$ and $\mu_e - r_e$ planes. Here n_b, M_V, r_e and μ_e are the Sérsic index, absolute V magnitude, scale radius and the average surface brightness within r_e, respectively. It is clear that J2345-0449 is located closer to pseudo bulges and far from classical bulge systems. However, the brightness of the bulge and r_e in J2345-0449 is higher than that shown for pseudo bulge disk galaxies in Fisher and Drory (Fisher & Drory 2008). Further evidence comes from the location of J2345-0449 in the $\langle\epsilon_b\rangle/\langle\epsilon_d\rangle-$ B/T plane (Figure 9), where ϵ_b and ϵ_d are the ellipticities of the bulge and disk. We found that our values for J2345-0449 closely matches with those of the pseudo bulge population, and the ratio of ellipticities ($\langle\epsilon_b\rangle/\langle\epsilon_d\rangle$) is higher than for classical bulges in galaxies of similar morphological T-type[4]. All the above checks strongly suggest that the central bulge in J2345-0449 should be classified as a pseudo-bulge, rather than a classical bulge. Consequently, evolution of the J2345-0449 host galaxy is probably governed by by quiet, 'secular evolution' processes in which disk instabilities drive gas to the center, rather than violent merger events that would have led to a classical bulge (Kormendy et al. 2010). This inference is further bolstered by the location of J2345-0449 in a sparse galactic environment, absence of any visible tidal debris (like tails, plumes or shells) and its well-developed spiral arms within a stable, rotationally supported stellar disk.

4. RESULTS: A SPIRAL HOST WITH EXTRAORDINARY PROPERTIES

The extreme nature of this spiral galaxy is underscored, firstly, by its unusual rotation curve. Rotation curves are the major tool for determining the mass distribution in spiral galaxies, e.g. (Sofue & Rubin 2001). The kinematics of the Balmer Hα line in the long-slit spectrum along the major axis, taken with the IFOSC on *IUCAA Girawali Observatory* 2m telescope, shows a rapidly rising rotational velocity in the inner $\sim$1 kpc, attaining an extremely large value, $V_{\rm rot} \sim 430$ kms^{-1} (inclination corrected) in

[4]T-type is a numerical value assigned visually to each class of galaxy in the De Vaucouleurs morphological classification scheme. T values run from -6 to +10, with negative numbers corresponding to early-type galaxies (ellipticals and lenticulars) and positive numbers to late types (spirals and irregulars). Spiral galaxies are assigned to a class based primarily on the tightness of their spiral arms, with larger T-value representing more open arms.

the asymptotic flat region at $r \gtrsim 10$ kpc from the galactic center (Sect. 3.5 and Figure 6). No kinematic signature of rotation is detected along the minor axis, which is a clear evidence for a planar, rotating galactic disk. Such rapid disk rotation ($V_{\rm rot} \sim 400 - 500$ kms^{-1}) is rare and has been reported earlier for just a few exceptionally massive spirals (e.g., Giovanelli et al. 1986; Rigopoulou et al. 2002; Akos et al. 2013). Assuming a quasi-spherical halo, the dynamical mass (luminous plus dark-matter) enclosed within a radius r is $M_{\rm dyn} = \kappa r V_{\rm rot}^2/G$, where κ is a correction factor, in range $0.6-1$ for a thin-disk to a spherical halo mass distribution model (Lequeux 1983), and G is the gravitational constant. We estimate $M_{\rm dyn} = 1.07(\pm 0.13) \times 10^{12} M_{\odot}$, for $\kappa = 1$ and $V_{\rm rot} \sim 430$ kms^{-1} at $r = 25$ kpc, i.e. $\sim$3.5 times the scale radius of the exponential disk. This places J2345-0449 amongst the brightest and most massive spirals known, having ~ 7 times the mass of the Milky Way within an equivalent radius, using the Tully-Fisher relation. Furthermore, we obtain its virial mass $M_{200} \sim 1.05 \times 10^{13} M_{\odot}$ and virial radius $R_{200} \sim 450$ kpc using the baryonic Tully-Fisher relation (BTFR) for ΛCDM cosmology (McGaugh 2005) ($M_{200} \propto V_{\rm rot}^{3.23}$) and scaling from M_{200} and $V_{\rm rot}$ (448 kms^{-1}) of the fast rotating spiral galaxy NGC 1961 (Akos et al. 2013).

Secondly, photometry and 2-D luminosity profile fitting of the CFHT and SDSS images showed that J2345-0449 is an extremely luminous (optical r-band: $M_r = -23.26$, near IR K-band: $M_K = -26.15$) isolated spiral galaxy (see above) lacking a spheroidal classical bulge, but having a compact disk-like 'pseudo-bulge' of low Sérsic index ($n \approx 1$) which contributes only $\sim$ 14% to the total g-band luminosity. In contrast, classical bulges generally have a more centrally peaked brightness profile characterized by a larger Sérsic index $n \approx 2$ - 5 (Fisher & Drory 2008). Recent recognition of a high fraction ($\sim$ 60%) of nearby spiral galaxies without a kinematically 'hot' central bulge challenges the conventional ideas of hierarchical galaxy formation; how so many bulgeless pure disk galaxies have come to exist, despite the galaxy mergers known to occur (Fisher & Drory 2008; Kormendy et al. 2010)? Below, we discuss this further, in the context of mass estimation of the central SMBH. J2345-0449 shows ongoing star forming activity across the galactic disk, traced by Hα and [N II] emission lines. It is also strongly detected by the *Galaxy Evolution Explorer* (GALEX) in the near (2316 Å) and far UV (1539 Å) bands (Martin et al. 2005), indicating a starburst of massive, hot O,B stars during the past $\sim$ 100 Myr. Interestingly, UV or Hα signatures of recent star formation ($\sim$ 100 Myr) are absent closer to the nucleus, showing only stellar population older than $\sim$ 1 Gyr (Figure 7). We interpret this as a result of heating and expulsion of the star forming medium by energetic, episodic feedback of the central AGN, as revealed by two pairs of radio lobes.

Another unusual property displayed by this disk galaxy is its exceptionally large stellar velocity dispersion of $\sigma_* = 379(\pm 25)$ km s^{-1} measured along its major axis, and $\sigma_* = 351(\pm 25)$ km s^{-1} along the minor axis, averaged within the central 2.35 kpc region (Sect. 3.6).

The slightly higher σ_* for the major axis possibly indicates some contribution from the disk rotation. Hence, we adopt the smaller σ_* of the minor axis as representative of the galaxy's central velocity dispersion. It is noteworthy that this dispersion value is significantly larger than that known for the majority of bulge-less disk galaxies on such a spatial scale (e.g., Hu 2008; Graham et al. 2011; Kormendy et al. 2011; Shankar et al. 2012), and compares well with that usually found for massive elliptical galaxies (e.g., Haring & Rix 2004; Marconi & Hunt 2003; Gultekin et al. 2009). This strongly hints at a large central concentration of mass, including a putative SMBH. We obtain the dynamical mass of the (pseudo) bulge $M_{\rm b} = 1.07(\pm0.14) \times 10^{11} M_{\odot}$, within one scale radius ($r_{\rm e} = 1.25$ kpc), and a black hole mass $M_{\rm BH} = 2.54(\pm0.48) \times 10^{8} M_{\odot}$ using the black hole mass vs. bulge mass correlation found by Marconi and Hunt (Marconi & Hunt 2003). This value is comparable to another estimate of $M_{\rm BH} = 3.88(\pm0.40) \times 10^{8} M_{\odot}$, obtained from the $M_{\rm BH} - \sigma_*$ correlation of Hu (Hu 2008) for the pseudo bulges. However if we use the $M_{\rm BH} - \sigma_*$ relation of Gultekin et al. (Gultekin et al. 2009), calibrated using a sample of both ellipticals and spirals, we obtain the black hole mass $M_{\rm BH} = 1.43 \times 10^{9} M_{\odot}$. Similarly, using K-band $M_{\rm BH} - L_K$ relation of Graham (Graham 2007), we obtain $M_{\rm BH} = 1.22 \times 10^{9} M_{\odot}$. Both these latter masses are close to each other, yet are significantly larger than the previous two mass estimates. We need to verify these rather large mass values via more direct and robust methods. If confirmed it would imply that J2345-0449 hosts a SMBH as massive as those found in giant elliptical galaxies, which is not expected for normal disk galaxies and is extremely unusual for a pure disk galaxy like J2345-0449 .

5. DISCUSSION

Despite lacking a classical bulge, this exceptional spiral galaxy is likely to host an unusually massive, accreting (radio-loud) black hole of $M_{\rm BH} > 10^{8}$ $M_{\odot}$. However our present data do not provide strong constraints on $M_{\rm BH}$, mainly because J2345-0449 lacks a classical bulge, whereas the black hole mass is more easily obtained from the tight $M_{\rm BH} - \sigma_*$ correlation in bulge dominated systems (Haring & Rix 2004; Marconi & Hunt 2003; Gultekin et al. 2009). For this reason the demographics of black holes in disk galaxies is poorly determined. However, there is growing evidence that a classical bulge is not essential for nurturing a massive black hole and some pseudo bulge systems may also host fairly massive black holes of masses $10^{3} - 10^{7} M_{\odot}$ (Kormendy et al. 2011; Shankar et al. 2012). Therefore these black holes must somehow attain masses substantially larger than the values implied by their bulge properties, possibly via a disk-driven, non-merger growth route. It appears that J2345-0449 is one such system, being an extreme member of such a population. Very little is known of the growth and AGN activity of super massive black holes in bulge-less spiral galax-

ies. Therefore, it would be a very significant result if more detailed observations show that J2345-0449 harbors a super massive black hole of $> 10^8$ $M_\odot$. We note that some previous works have suggested (e.g., Hu 2008; Graham et al. 2011; Shankar et al. 2012), that pseudo bulge and barred galaxies may host black holes that are about 3 to 10 times less massive than pure ellipticals having the same σ_*. It has also been proposed that their black hole masses do not correlate well with properties of galaxy disks or their pseudobulges (Kormendy et al. 2011), and hence the growth process of massive black holes in flattened galactic disks lacking prominent bulges is still mysterious and a subject of intense debates and investigations (Shankar et al. 2012; Kormendy et al. 2011; Simmons et al. 2013).

Our estimation of black hole mass in J2345-0449 could be a lower limit, constrained by the lack of sub-arcsec resolution spectral data. Nevertheless, it is interesting to note that the lower range of our estimated black hole mass (2 - 4 $\times 10^8$ $M_\odot$) is close to the minimum required for the production of large-scale relativistic jets in radio galaxies and quasars (Laor 2000; Gopal-Krishna et al. 2008; Sikora et al. 2007; Chiaberge & Marconi 2011). At the present stage one can not rule out an even more massive black hole of $\gtrsim 10^9$ $M_\odot$ in this galaxy, given its extreme radio properties and exceptionally large mass. Therefore, a more robust and direct estimate of the black hole mass in J2345-0449 is needed, possibly via spatially resolved stellar kinematics or gas dynamics measurements close to its gravitational sphere of influence: $r_g \sim 50\,(M_{\rm BH}/10^9\,M_\odot)(\sigma_*/300\,{\rm km\,s^{-1}})^{-2}$ pc $\equiv 0.035'' - 0.35''$ for $M_{\rm BH} \sim 10^9 - 10^{10} M_\odot$. At ~ 340 Mpc distance ($1'' \equiv 1.43$ kpc) such a refined measurement is challenging if $M_{\rm BH} \lesssim 10^9 M_\odot$, requiring very high ($\sim 0.01''$) spatial resolution. Nevertheless, this method has recently revealed a $1.7 \times 10^{10} M_\odot$ extra-massive black hole in the nearby galaxy NGC 1277, another fast rotating, disk galaxy with a pseudo-bulge (Van den Bosch et al. 2012). Interestingly, for NGC 1277 the stellar velocity dispersion is ~ 333 km s^{-1} at the half light radius ($2.8''$) – very close to the present case – which rises to > 400 km s^{-1} near the black hole's sphere of influence. Therefore, it is tempting to speculate that J2345-0449 might also harbor an extremely massive black hole, that would help to explain its unusual radio properties, further discussed below.

Because it is not obvious how this galaxy acquired such a range of extraordinary properties, it poses challenges to theoretical models and holds important clues for understanding the co-evolution of black holes and disk galaxies, accretion physics, the formation of large scale relativistic jets in AGN, and a possible solution to the long standing puzzle of why disk galaxies are nearly universally devoid of powerful double radio sources. We propose that this spiral galaxy's huge mass, angular momentum, and episodic radio jet ejection are all the results of its rare, unusual evolutionary history that has led to the formation of both a rotationally supported massive, fast-spinning galactic disk (here $(V_{\rm rot}/\sigma_*)^2 \sim 1.5$), as well as a mass accereting, possibly rapidly spinning, unusually massive central SMBH.

Very little is known about the formation and evolution of such extremely massive spiral galaxies, as they are found rarely and hardly ever known to eject powerful relativistic jets on Mpc scale like J2345-0449 . The cosmic evolution of the galactic disk of J2345-0449 may have been primarily driven by external cold gas accretion and internal 'secular' processes instead of recent ($t \lesssim$ few$\times 10^9$ y) major merger events. This is suggested by its disk-like pseudo-bulge, absence of close galactic neighbours and of tidal debris (e.g., stellar streams, plumes or shells), and by its stable, rotationally supported massive stellar disk showing well formed spiral arms. Furthermore, a close alignment (within ~ 10 degree) of the inner and outer radio-lobe pairs implies that the black hole's spin axis – which in equilibrium orients itself orthogonal to the inner accretion disk due to the Lense-Thirring frame dragging effect (Bardeen & Petterson 1975)– has remained stable (non precessing), at least between the two last episodes of jet triggering on timescales of $t \sim 10^8$ y. All this suggests that the galactic disk and its central black hole might have a quiet evolution together, without major mergers. The massive galactic disk is clearly rotationally supported ($(V_{\rm rot}/\sigma_*)^2 \sim 1.5$) and should be dynamically stable against gravitational instability.

The formation epoch of J2345-0449 probably also lies in the early universe (redshifts $z \gtrsim 2-3$) more than 10 Gyr ago, i.e. during the era of galaxy formation and quasar activity. In that era, most galactic disks (pancakes) were unvirialized, still assembling around isolated halos via minor mergers and mass accretion from cool, gas-rich filaments of the cosmic-web, and often experiencing high star formation rates of $\sim 10^2 - 10^3\ M_\odot {\rm yr}^{-1}$. The initial build up of the present large large mass and angular momentum of the galactic disk of J2345-0449 possibly started very early (probably $z \gtrsim 6$) during the pancake stage of its parent halo, via gravitational tidal torques and rapid disk feeding through a few dominant, coplanar cold-streams ('cold mode' accretion), as recently observed for a star forming disk galaxy at $z = 2.3$ (Bouche et al. 2013) and also shown in numerical simulations (Keres et al. 2005; Governato et al. 2007; Dekel et al. 2009; Danovich et al. 2012). For very massive halos of mass $\gtrsim 10^{12} M_\odot$, another 'hot mode' growth also takes place via the intergalactic gas accreting quasi-spherically, experiencing an accretion shock and heating to virial temperature as it collides with the hot, hydrostatic halo near the virial radius, and then being accreted onto the galaxy on radiative cooling time scale (Keres et al. 2005; OcVirk et al. 2008). Simultaneously, the growth of the massive black hole of this bulge-less spiral possibly started from an initial 'seed' black hole mass, via an internal disk-driven (secular) accretional route - through a rapid phase of mass and angular momentum (spin) transfer from a gas-rich accretion disk fed at high Eddington rate (Berti & Volonteri 2008). Its inner accretion zone was coupled to the fast-spinning outer galactic disk via the viscous and magnetic torques. This coherent growth process would spin-up the growing black hole to a high value if copious fuel supply is available for a long enough time; in contrast to the low final spin expected in a stochastic (i.e.

chaotic or incoherent) merger driven growth scenario (Dotti et al. 2013; Dubois et al. 2014). It is well known that a black hole approximately doubling its mass by accreting a constant angular momentum gas from a standard thin-disk would acquire a maximum 'canonical' spin of $a = 0.998$ (Thorne 1974) due to a braking torque, where the dimensionless spin parameter is $a = cJ_{\rm BH}/GM_{\rm BH}^2$ and black hole's angular momentum is $J_{\rm BH}$. Such a massive, acccreting-spinning black hole would be a highly efficient 'engine' for launching, fast, collimated plasma jets via the Blandford-Znajeck mechanism (or variants of it), further boosted by a strong build up of magnetic flux near the black hole horizon by advection of the accretion flow. Below we further comment on the feasibility and implications of such a SMBH growth and jet formation process in J2345-0449 .

Obviously, the most striking property that sets J2345-0449 apart from nearly all other spiral galaxies (including Seyferts) is its large mass and unusual radio loudness, resulting from highly efficient ejection of relativistic jets on Mpc scale. The extreme rarity of such galaxies implies that whatever physical process that created such huge radio jets in J2345-0449 must be very difficult to realize and maintain for long periods of time in most other spiral/disk galaxies. Thus an important question is; what could be responsible for the efficient fuelling and sustained collimated jet ejection activity in J2345-0449 ? The answer requires a very detailed knowledge of the properties of its central black hole engine, i.e. its mass, spin and the nature of its accretion flow, viz., the mass accretion rate and the magnetic field topology of the inner accretion disk, most of which is clearly lacking at present. Although the exact mechanism of jet launching is not known for J2345-0449 , a promising and widely accepted explanation is the Blandford-Znajek process that efficiently extracts the rotational energy of the black hole and the orbital energy of the accretion flow into an intense outflow of Poynting flux dominated electromagnetic jet. In the Blandford-Znajek process the jet launching requires a massive, spinning Kerr black hole, and an accretion disk threaded with strong poloidal magnetic field lines advected near the hole's outer horizon at radius $R_{\rm H} = (GM_{\rm BH}/c^2)[1 + (1 - a^2)]^{1/2}$. In the classic BZ process the electromagnetic luminosity of jet $\bar{Q}$ scales with black hole properties as

$$\bar{Q}_{44} \approx 0.2\, M_8^2\, a^2\, B_4^2, \tag{9}$$

where, $\bar{Q}_{44} = \bar{Q}/10^{44}$ erg s^{-1}, the black hole mass $M_8 = M_{\rm BH}/10^8 M_\odot$ and the poloidal magnetic field $B_4 = B/10^4$ Gauss (Blandford & Znajek 1977; MacDonald & Thorne 1982; Tchekhovskoy et al. 2010; Sadowski et al. 2013; Penna et al. 2013). Thus, the jet power depends strongly on the black hole mass, spin and the magnetic flux at the horizon. This prediction is confirmed by recent numerical general relativistic magnetohydrodynamic (GRMHD) simulations which show that the efficiency (η) of conversion of accretion luminosity to the jet

luminosity (including a possible coronal wind) could be as high as $\eta = (\bar{Q}/\dot{M}c^2) \sim 30-140\%$ for spin $a = 0.5 - 0.99$, if the magnetized accretion flow manages to accumulate (via advection and turbulent amplification) large magnetic flux near the black hole's horizon (Tchekhovskoy et al. 2010; Tchekhovskoy et al. 2011; Penna et al. 2013). Similar results have been found by Hawley and Krolik (Hawley & Krolik 2006) which demonstrate that the electromagnetic extraction of the spin energy of a black hole is very much feasible.

Observationally, the jet kinetic power ($\bar{Q}$) is a key descriptor of the state of an accreting SMBH system; its mass, spin and the magnetic field of the accretion disk. Correlation of low-frequency ($\nu \sim 150$ MHz) radiative radio power of FRII radio sources against their jet power shows that the radio luminosity of the jet constitutes only a small fraction ($< 1\%$) of the total kinetic power output (Punsly & Zhang 2011; Daly et al. 2012). Here we use the low frequency radio flux, which usually originates in diffuse, optically thin radio lobes moving at low velocities, thus the relativistic beaming effects are negligible. We estimate the 151 MHz lobe flux density to be 15.75 Jy (excluding the inner jet/lobe pair and the core) using the 0.3 GHz and 1.4 GHz measurements and the observed radio spectral index $\alpha = 2$. Using the published calibration relations (Punsly & Zhang 2011; Daly et al. 2012) we obtain $\bar{Q} \approx 1.7 \times 10^{44}$erg s^{-1} for the (time-averaged) jet kinetic power in J2345-0449 . A similar value of $\bar{Q}$ is obtained using the relation for estimating the total jet power from radio power, for a $M_{\rm BH} \sim 10^8 M_\odot$ (equation 1 in Meier 2001). As we have applied no correction for the (unknown) energy loss in the outer radio lobes, $\bar{Q}$ is likely to be a lower limit. This high value of $\bar{Q}$ in J2345-0449 is typical of high powered FR II jets found in radio loud quasars (Punsly & Zhang 2011) and is above the FR I/FR II divide at $\bar{Q} \approx 5 \times 10^{43}$erg s^{-1}, suggestive of a highly efficient supersonic jet ejection (Rawlings & Saunders 1991), energetic enough to pierce through the host galaxy's dense environment.

Therefore, assuming $M_{\rm BH} \sim 2 \times 10^8 M_\odot$, the lower of the aforementioned black hole mass estimates for J2345-0449 , and assuming a rather strong magnetic field $B = 2 \times 10^4$ Gauss, equation 9 above shows that the estimated jet power can be achieved via the classic (MHD dominated) BZ process for $a \gtrsim 0.73$, i.e. needing a rapid, yet not a maximally spinning black hole. However, even if this black hole is near maximally spinning ($a = 0.98$), the magnetic field cannot be lower than $B \approx 1.5 \times 10^4$ Gauss, highlighting the key role of magnetic field advection in extracting the spin energy of the hole. It is also evident that for the same black hole mass as above, but for a very low spin $a \approx 0.1$, the estimated $\bar{Q}$ is not obtained unless the disk magnetic field $B \gtrsim 1.5 \times 10^5$ Gauss. However, such an extremely strong magnetic field might never occur normally, as the field strength near the inner accretion disk is not expected to exceed the Eddington value $B_{Edd} \approx 6 \times 10^4 \, M_8^{-1/2}$ Gauss for accretion at the Eddington rate. From mid-IR colors, lack of broad lines and a very weak Hα flux observed in the AGN's optical spectrum, we inferred above that the accretion state of black hole in

J2345-0449 is possibly sub-Eddington. This is a characteristic of a radiatively inefficient, low luminosity active galactic nuclei (LLAGN/LINER). Thus, the above analysis suggests that in the launching of highly efficient jetted outflow in J2345-0449 the spin of the black hole and its accretion state might be playing dominant roles, and additionally, the black hole is required to be unusually massive, despite being hosted by a spiral galaxy. We point out that compared to pure BZ process, mainly considered here for its simplicity, some more complex hybrid models of jet production, based on a combination of Blandford-Payne (Blandford & Payne 1982) and Blandford-Znajek mechanisms (Blandford & Znajek 1977) have been proposed (e.g., Meier 2001; Nemmen et al. 2007) which predict higher jet luminosities under similar physical conditions.

Is such a rare combination of unusually high black hole mass, spin and low accretion state achievable in a bulge-less disk galaxy? Recent numerical simulations (Dotti et al. 2013) of black hole growth (via accretion and mergers) predicts that at low redshifts the most rapidly rotating black holes ($a > 0.9$) are also the most massive ones ($10^8 - 10^9 M_\odot$), and their spin orientation remain stable over many accretion cycles. However, such a black hole generally ends up in an elliptical galaxy and not in a pure spiral, contrary to the present case. For this to happen in a spiral galaxy like J2345-0449 would require a coherent, high rate of mass accretion, whereby the black hole grows rapidly and is spun-up via matter accreted with a well defined, almost constant angular momentum direction, instead of major mergers. Due to this unusual evolutionary route, the fundamental correlations of the black hole mass and galaxy properties observed in bulge dominated systems are unlikely to hold in the present case. Future studies might further explore this important aspect in this and similar systems. It is especially important to verify if the black hole in J2345-0449 is indeed more massive than the minimum value ($\sim 10^8 - 10^9 M_\odot$) inferred in several works for the development of powerful radio jets in AGN (e.g., Laor 2000; Gopal-Krishna et al. 2008; Sikora et al. 2007; Chiaberge & Marconi 2011). Such a large black hole mass will pose a challenge for the models of growth of black holes in disk galaxies. Our ideas can be better tested when in future more accurate measurements of both the mass and spin of the black hole in J2345-0449 become available.

It seems plausible that the unusual jet activity of J2345-0449 may have been triggered by the AGN accretion state switching from a previous high Eddington rate ($\lambda \gtrsim 10^{-2} - 10^{-3}$) to a sub-Eddington rate, where

$$\lambda = \dot{M}/\dot{M}_{Edd} \tag{10}$$

denotes the dimensionless mass accretion rate in units of the Eddington accretion rate $\dot{M}_{Edd}$. A strong link between jet formation and accretion rate has been discussed in the

literature (e.g., Rees et al. 1982; Meier 2001), which is of direct relevance in the context of the giant radio jets found in this unusual spiral galaxy. It is well known that at accretion rates above a critical value $\lambda_{\rm crit} \sim 10^{-2} - 10^{-3}$ the disk structure is a standard Shakura and Sunyaev, radiatively efficient, geometrically thin disk (Shakura & Sunyaev 1973), whereas at reduced accretion rates ($\lambda << \lambda_{\rm crit}$), transition to an advection-dominated accretion flow (ADAF) results, fueled by hot gas from a large-scale quasi-spherical halo (Narayan & Yi 1994; Narayan & Yi 1995). In ADAF most of the heat generated by the local, turbulent viscous heating is rapidly advected inside the black hole horizon (and eventually swallowed) or released in a wind or radio-jet. Thus, the radiative cooling efficiency of the geometrically thick, optically thin, disk is greatly diminished. Therefore, one would find black holes in ADAF state to be unusually faint (disk bolometric luminosity $L_{bol} << 0.1\dot{M}c^2$); such as the galactic center black hole Sgr A* or the radio galaxy M87/Virgo-A (Falcke et al. 2004). In ADAF the inner region of the accretion disk gets extremely hot, forming a thick ion-torus which helps to collimate the relativistic outflow into the 'funnel' regions at the poles (Rees et al. 1982). In addition, the thick torus effectively anchors strong poloidal magnetic field that is required to channel the rotational energy of the hole in the form of electromagnetic fields and particles via the BZ mechanism (Beckwith & Hawley 2008). The magnetic field plays another important role as MHD turbulence in accretion flow is generated by the magnetorotational instability (Balbus & Hawley 1991) which provides the necessary viscous torque for removing angular momentum from the accreting gas, thus driving the inflow, and amplifying the large-scale magnetic field.

This is an attractive scenario for J2345-0449 because the AGN in it is presently in the low excitation state (LERG/LLAGN), showing extremely low radiative efficiency, but a very high kinetic luminosity in jetted outflows, strongly reminiscent of an ADAF. This observation provides an important clue as to how the radio jets in J2345-0449 might be launched. We further investigate this rare occurrence of relativistic jets in light of the fundamental paradigm, that, inspite of a vast difference in involved black hole mass, length and time scales, almost all relativistic disk-jet coupled phenomena happen in a scale invariant manner in both radio loud AGNs and the galactic 'microquasars' (Mirabel & Rodriguez 1994). In galactic black hole X-ray binaries a transition to 'low-hard' X-ray state is generally always accompanied by steady radio jet formation, whereas their radio emission is quenched in 'high-soft' X-ray state (Fender et al. 2004). This indicates a strong link between the jet formation and accretion state of a black hole. In this context a 'fundamental plane' (FP) of accreting black holes which links SMBHs to stellar mass galactic black holes has been proposed, finding a positive correlation between their core radio ($L_{\rm R}$) and X-ray ($L_{\rm X}$) luminosities, with the black hole mass as a scaling factor, of the form (Merloni et al. 2003; Falcke et al. 2004)

$$log L_{\rm R} = 0.60\, log L_{\rm X} + 0.78\, log M_{\rm BH} + 7.33 \tag{11}$$

Where $L_{\rm R}$ (at 5 GHz) and $L_{\rm X}$ (in 2-10 KeV band) are in erg s^{-1} and the black hole mass is in $M_\odot$ units. The FP is a powerful scheme which unifies the physics of accretion and jet formation for black holes across an enormous $\sim 10^1 - 10^{10}\, M_\odot$ mass range, primarily in their sub-Eddington, low-hard state. At present we lack a hard X-ray flux and a robust mass estimate for black hole in J2345-0449 to place it on the FP. Nevertheless, assuming central black hole mass is in range of $10^8\, M_\odot$ to $10^9\, M_\odot$, the above FP relation predicts a core X-ray luminosity $L_{\rm X} \sim 2.4 \times 10^{43}$ erg s^{-1} to $L_{\rm X} \sim 1.2 \times 10^{42}$ erg s^{-1} respectively, using the VLA 5 GHz core (the jet-base) radio luminosity of $L_{\rm R} \sim 4 \times 10^{39}$ erg s^{-1}. Therefore, a future measurement of $L_{\rm X}$ via X-ray observations, and an independent estimate of the black hole mass would reveal if the AGN in J2345-0449 (putatively in a low-hard ADAF state) conforms to the FP of accreting black holes or not? Such data will provide a powerful means of testing the disk-jet coupling theories in an extremely unusual circumstance, and may also suggest some new, hitherto untested ways of forming relativistic jets. However, the fundamental question remains; why such a transition of accretion state does not commonly occur in other spiral galaxies, which almost never show extended radio jets and are mostly radio-quiet? As we have discussed above, the answer could be, that perhaps in our present galaxy the efficiency of jet-launch is greatly boosted by an unusually massive (and possibly rapidly spinning) SMBH (at least a few $\times 10^8 M_\odot$) in the galaxy's nucleus, formed via a predominantly disk driven accretion route. Moreover, a strong, almost saturated magnetic field lines anchoring the accretion disk might have also enhanced the luminosity of the jet, which can take place only via a geometrically thick ADAF (Sikora & Begelman 2013). Moreover, in the ADAF, unlike the thin-disk case, the black hole spin is a crucial factor for powerful jet formation (Meier 2001; Tchekhovskoy et al. 2010; Sadowski et al. 2013).

Such an over-massive, spinning black hole in a pure (spheroidal bulgeless) disk galaxy can result only via a previous rapid growth phase at high mass accretion rate $\lambda \sim 0.1 - 0.01$. In this formative phase, now long past, the galaxy J2345-0449 might have shone like a luminous quasar due to large radiative efficiency of a strongly accreting thin disk. In accretion models, the radiative efficiency and growth rate of black hole depends only on the dimensionless parameter λ and not on the absolute value of M or $\dot{M}$. The e-folding black hole growth time $t_{\rm BH}$ and the black hole mass at a given time M(t) are given by (Shapiro 2005; Hopkins et al. 2006)

$$t_{\rm BH} = M/\dot{M} = t_{\rm sal}/\lambda \tag{12}$$

$$M({\rm t}) = M(0) \exp[\, ((1-\epsilon)/\epsilon)\, (t/t_{\rm sal})\, \lambda\,] \tag{13}$$

where, the Salpeter time-scale $t_{\rm sal} = 0.45$ Gyr, initial black hole seed mass $M(0)$ at $t = 0$ and the radiative efficiency of the accreted mass into energy $\epsilon \approx 0.06 - 0.42$ (for spin $a = 0 - 1$). With gradual mass and angular momentum transfer and a steady increase of the black hole spin a, the radiative efficiency ϵ would also rise (for a radiatively efficient disk), slowing down the black hole growth rate. Thus, in the initial phase of black hole growth the mass accretion rate needs to be near Eddington ($\lambda \sim 1$) and the spin-up rate $\dot{a}$ slow so that the black hole may grow to an unusually large final mass via gaseous accretion. We have no estimate for the initial seed mass of the black hole in J2345-0449 and the cosmic history of its spin and mass evolution is also unknown. Nevertheless, starting from a Population-III (POP-III) seed black hole of $M(0) \sim 10^2 M_{\odot}$, formed via stellar route at $z \approx 40$, and a coherent, average high Eddington rate accretion ($\bar{\lambda} \approx 0.1$, $\bar{\epsilon} = 0.1$), it still requires ~ 18 e-folding times of $t \approx 18 \times t_{\rm sal} \approx 8$ Gyr ($z(t) \approx 0.6$) to grow a black hole to $\sim 10^9 M_{\odot}$ (equation 13). However, this is shortened to $t \approx 1.8 \times t_{\rm sal} = 0.8$ Gyr (by $z(t) \approx 6.8$) for near-Eddington rate accretion ($\bar{\lambda} \approx 1$). For significantly lower accretion rates ($\lambda << 1$) the growth timescale becomes longer than the age of the universe and the black hole cannot possibly accumulate a significant fraction of its mass. Thus, a relatively short, initial phase of rapid growth of the central black hole at near Eddington rate accretion is suggested for J2345-0449 , implying that presently we are observing its AGN as a faded remnant of an erstwhile highly luminous QSO phase.

Therefore, in our proposed model, the radio-jet launching spiral galaxy J2345-0449 finds itself in an accretion state similar to local radio loud ellipticals of low excitation state, in contrast to the recently discovered radio loud, narrow-line Seyfert-1 AGN in spiral galaxies (extreme objects themselves) that are inferred to be accreting at near Eddington rates ($\lambda \approx 0.1 - 1$), host smaller mass black holes ($M_{\rm BH} \sim 10^6 - 10^8 M_{\odot}$) and are never observed to eject $0.1 - 1$ Mpc scale relativistic jets (Doi 2012; Foschini 2011; Komossa et al. 2006). Moreover, existence of this galaxy is at odds with the finding that among the AGN population in local Universe essentially all AGN with moderate to large accretion rates (i.e., $t_{\rm BH} < t_{\rm Hubble} \sim 14$ Gy) are in spirals, whereas their counterparts in almost every elliptical have a negligible mass accretion rate ($t_{\rm BH} > t_{\rm Hubble}$) (Hopkins et al. 2006). In J2345-0449 an accretion rate-dependent state transition to low radiative efficiency, ADAF state might have taken place due to the enormous growth of its accreting black hole itself and its energetic feed-back acting on the accretion flow, heating the latter and thus reducing the AGN fuelling rate below the critical value $\lambda_{\rm crit} \sim 10^{-2} - 10^{-3}$. The two set of radio lobes forming the double-double structure are clearly indicative of an intermittent radio jet activity, possibly resulting from an episodic switching of the accretion modes between a low (ADAF, powerful radio jets, low radiative efficiency) to high (thin disk, no/weak radio jets, high radiative efficiency) accretion states. Thus, finding the black hole's mass, spin, and the impact of the highly energetic jet

outflow on the surrounding galaxy is clearly very important. Perhaps, the most crucial clues for understanding this extraordinary and puzzling radio galaxy would come from its future detailed X-ray, UV, infra-red and radio observations. This will allow the complete spectral energy distribution of the galaxy and central AGN to be determined for theoretical modelling. A sensitive X-ray observation of a possible corona of hot, X-ray emitting gas around the massive spiral host, a remnant of its formation history, and detection of an AGN with hard X-ray spectrum (peaking at ~ 100 keV) showing low bolometric luminosity would strengthen the model outlined above. The spin of the black hole can be determined by the method of continuum fitting the flux and temperature of the X-ray emission from the accretion disk, while the mass of the black hole can be obtained via high resolution stellar spectroscopy near the black hole's sphere of influence. High resolution VLBI imaging and polarization mapping of the inner radio jets near the core, in the disk/corona collimation region, would also be very informative for understanding the jet launching process in this highly unusual AGN.

To conclude, the present object J2345-0449 is the most extreme example of powerful jet activity and SMBH growth in a spiral galaxy, probably arising via a non-standard evolutionary route that mainly involves internal, merger-free processes persisting through most of its formation history. Future observations and numerical simulations should clarify whether its exceptional properties can be understood within the current frameworks of galaxy formation.

On the occasion of 50 years of radio astronomy research at the Tata Institute of Fundamental Research (TIFR) and India, as well as 10 years of operation of the Giant Metrewave Radio Telescope (GMRT) as an international observatory, we dedicate this work to the vision and pioneering spirit of Professor Govind Swarup, late Professor Vijay Kapahi and many talented Indian scientists, engineers and technicians who have made it possible. We thank the anonymous referee for providing many constructive comments which improved the paper. We thank IUCAA Girawali Observatory (IGO) staff, and Prof. Vijay Mohan for their support during observations. Team members of IFOSC instrument on the IUCAA 2m telescope are thanked for their excellent work. J.J. and BKG acknowledge IUCAA's support under the Visiting Associate program. We used archival data from GMRT, CFHT and VLA facilities. The GMRT is a national facility operated by the National Centre for Radio Astrophysics (NCRA) of the Tata Institute of Fundamental Research, India. Our results are based on observations obtained with MegaCam, a joint project of CFHT and CEA/DAPNIA, at the Canada-France-Hawaii Telescope, which is operated by the National Research Council of Canada, the Institut National des Science de l'Univers of the Centre National de la Recherche Scientifique of France and the University of Hawaii. The VLA is a facility of the National Radio Astronomy Observatory (NRAO). The NRAO is a facility

of the National Science Foundation, operated under cooperative agreement by Associated Universities, Inc. Funding for SDSS has been provided by the Alfred P. Sloan Foundation, the Participating Institutions, the National Science Foundation, and the U.S. Department of Energy Office of Science.

REFERENCES

Abdo, A.A., Ackermann, M.,Ajello, M., et al. 2009, ApJ **707**, L142

Ahn, C.P. et al. 2014, ApJS **211**, 16

Ákos, B., Forman, W.R., Kraft, R.P. & Jones, C., 2013, ApJ **772**, 98

Alexander, D.M. & Hickox, R.C., 2012, *New Astronomy Reviews* **56**, 93

Argence, B. & Lamareille, F. 2009, A&A **495**, 759

Balbus, S.A. &Hawley, J.F. 1991, ApJ **376**, 214

Baldwin, J.A., Phillips, M.M. & Terlevich, R. 1981, *PASP* **93**, 5

Bardeen, J.M.& Petterson, J.A. 1975, *ApJL* **195**, L65

Beckwith, K. &Hawley, J.F. 2008, ApJ **678**, 1180

Begelman, M.C., Blandford, R.D., Rees, M.J. 1984, *Rev. Mod. Phys.* **56**, 255

Berti, E. & Volonteri, M. 2008, ApJ **684**, 822

Bertin, E. & Arnouts, S. 1996, A&AS **117**, 393-404

Bertin, E., Mellier, Y., Radovich, M., Missonnier, G., Didelon, P. & Morin, B. 2002, *Astr. Soc. Pacific Conf. Ser.*, **281**, 228 (Edited by David A. Bohlender, Daniel Durand, and Thomas H. Handley)

Blandford, R.D. & Znajek, R.L. 1977, MNRAS **179**, 433

Blandford, R.D. &Payne, D.G. 1982, ApJ **199**, 883

Bouche, N.,Murphy, M.T.,Kacprzak, G.G., et.al. 2013, *Science* **341**, 50

Boulade, O., et al. 2003, *Society of Photo-Optical Instrumentation Engineers (SPIE) Conference Series* **4841**, 72

Cappellari, M. & Emsellem, E. 2004, *PASP* **116**, 138

Chiaberge, M. & Marconi, A. 2011, MNRAS **416**, 917

Courteau, S. 1997, AJ **114**, 2402

Daly, R.A.,Spinkle, T.B.,O'Dea, C.P,et.al. 2012, MNRAS **423**, 2498

Dekel, A.,Birnboim, Y.,Engel, G., et al. 2009,*Nature* **457**, 451

Danovich, M.,Dekel, A.,Hahn, O.& Teyssier, R. 2012, MNRAS **422**, 1732

Doeleman, S.S.,Fish, V.L.,Schenck, D.E., et al. 2012, *Science* **338**, 355

Doi, A.,Nagira, H.,Kawakatu, N., et al. 2012, ApJ **760**, 41

Dotti, M., Colpi, M., Pallini, S., Perego, E. & Volonteri, M. 2013, ApJ **762**, 68

Dubois, Y., Volonteri, M., Silk, J., Devriendt, J. & Slyz, A. 2014, MNRAS **440**, 2333

Dunlop, J.S., Mclure, R.J., Kukula, M.J., Baum, S.A., O'Dea, C.P. & Huges, D.H. 2003, MNRAS **340**, 1095

Falcke, H., Kording, E. & Markoff, S. 2004, A&A **414**, 895

Fanaroff, B.L., & Riley, J.M. 1974, MNRAS **167**, 31P

Fender, R.P., Belloni, T.M. & Gallo, E. 2004, MNRAS **355**, 1105

Fisher, D.B. & Drory, N. 2008, AJ **136**, 773

Foschini, L. 2011, *Res. in Astron. Astroph.* **11**, 1266

Gadotti, D.A. 2009, MNRAS **393**, 1531

Gebhardt, K., et al. 2000, ApJ **539**, L13

Giovanelli, R.,Haynes, M.P.,Rubin, V.C. &Ford Jr., W.C. 1986, ApJ **301**, L7

Gopal-Krishna, Mangalam, A. & Wiita, P.J. 2008, ApJ **680**, L13-L16

Governato, F.,Willman, B.,Mayer, L., et al. 2007, MNRAS **374**, 1479

Graham, A.W. 2007, MNRAS **379**, 711

Graham, A.W., Onken, C.A., Athanassoula, E. & Combes, F. 2011, MNRAS **412**, 2211

Gultekin, K., Richstone, D.O., Gebhardt, K., et al. 2009, ApJ **698**, 198

Gurkan, G, Hardcastle, M.J. & Jarvis, M.J.. 2014, MNRAS **438**, 1149

Gwyn, S.D.J. 2008, *PASP* **120**, 212

Hawley, J.F. & Krolik, J.H. 2006, ApJ **641**, 103-116

Haring, N. & Rix, Hans-Walter, (2004), ApJ **604**, L89

Hopkins, P.F., Narayan, R. &Hernquist, L. 2006, ApJ **643**, 641

Hota, A.,Sirothia, S.K.,Ohyama, Y., et al. 2011, MNRAS **417**, L36

Hu, Jian 2008, MNRAS **386**, 2242

Jones, D., et al. 2009, MNRAS **399**, 683

Kennicut, R.C. (Jr.) 1992, ApJ **388**, 310

Keres, D., Katz, N., Weinberg, D.H, & Davé, R. 2005, MNRAS **362**, 2

Komossa, S., et al 2006, AJ **132**, 531

Kormendy, J. & Richstone, D. 1995, *Ann. Rev. Astron. Astroph.* **33**, 581

Kormendy, J., Drory, N., Bender, R., & Cornell, M.E. 2010, ApJ **723**, 54

Kormendy, J., Bender, R. & Cornell, M.E. 2011, *Nature* **469**, 374

Laor, A. 2000, ApJ **543**, L111-L114

Ledlow, M.J., Owen, F.N. & Keel, W.C.. 1998, ApJ **495**, 227

Lequeux, J. 1983, A&A **125**, 394

Lynden-Bell, D. 1969, *Nature* **223**, 690

MacDonald, D. & Thorne, K.S. 1982, MNRAS **198**, 345

Machalski, J., Koziel-Wierzbowska, D. & Jamrozy, M. 2007, *Acta Astronomica* **57**, 227

Magorrian, J. et al. 1998, ApJ **115**, 2285

Marconi, A. & Hunt, L.K., 2003, ApJ **589**, L21

Martin, D.C. et al. 2005, ApJ **619**, L1

McGaugh, S.S. 2005, ApJ **632**, 859

Meier, D.L. 2001, ApJ **548**, L9

Merloni, A., Heinz, S. & De Matteo, T. 2003, MNRAS **345**, 1057

Mirabel, F. & Rodriguez, L.F. 1994, *Nature* **371**, 46

Morganti, R. et al. 2011, A&A **535**, A97

Narayan, R. &Yi, Insu 1994, ApJ **428**, L13

Narayan, R. &Yi, Insu 1995, ApJ **452**, 710

Nemmen, R. S., Bower, R. G., Babul, A. & Storchi-Bergmann, T. 2007, MNRAS **377**, 1652

OcVirk, P., Pichon, C., & Teyssier, R. 2008 MNRAS **390**, 1326

Peng, C. Y., Ho, L. C., Impey, C. D. & Rix, H.-W. 2002 AJ **124**, 266

Penna, R.F., Narayan, R. & Sadowski, A. 2013, MNRAS **436**, 3741

Pettini, M. & Pagel, B.E.J. 2004, MNRAS **348**, L59

Poggianti, B. M. 1997, A&AS **122**, 399-407

Punsly, B. & Zhang, H. 2011, ApJ **735**, L3

Rawlings, S. & Saunders, R. 1991, *Nature* **349**, 138

Rees, M.J., , Blandford, R.D. & Phinney, E.S. 1982, *Nature* **295**, 17

Rigopoulou, D.,Franceschini, A.,Aussel, H.,et.al. 2002, ApJ **580**, 789

Sadowski, A., Narayan, R., Penna, R.F. & Zhu, Y. 2013, MNRAS **436**, 3856

Saikia, D.J., & Jamrozy, M. 2009, *Bull. Astron. Soc. India* **37**, 63

Schlegel, D. J., Finkbeiner, D. P. & Davis, M. 1998, ApJ **500**, 525

Schoenmakers, A.P.,de Bruyn, A.G.,Rottgering, H.J.A., van der Laan, H.,& Kaiser, C.R. 2000, MNRAS **315**, 371

Schwope, A. et al. 2000, *Astronomische Nachrichten* **321**, 1

Shakura, N.L. & Sunyaev, R.A. 1973, A&A **24**, 337

Shankar, F., Marulli, F., Mathur, S., Bernardi, M. & Bournaud, F. 2012, A&A **540**, A23

Shapiro, S.L. 2005, ApJ **620**, 59-68

Sikora, M., Stawarz, L. & Lasota, Jean-Pierre 2007, ApJ **658**, 815

Sikora, M. & Begelman, M.C. 2013, ApJ **764**, L24

Simmons, B.D.,Lintott, C.,Schawinski, K., et al. 2013, MNRAS **429**, 2199

Sofue, Y. & Rubin, V.C. 2001, *Ann. Rev. Astro. Astrophys.* **39**, 137

Soltan, A. 1982, MNRAS **200**, 115

Stern, D., et al. 2012, ApJ **753**, 30

Tchekhovskoy, A., Narayan, R. & McKinney, J.C. 2010, ApJ **711**, 50

Tchekhovskoy, A., Narayan, R. & McKinney, J.C. 2011, MNRAS **418**, L79

Thorne, K.S. 1974, ApJ **191**, 507

van den Bosch, R.C.E.,Gebhardt, K., Gultekin, K.,et al. 2012, Nature **491**, 729

Vazdekis, A. 1999, ApJ **513**, 224

Vikram, V.,Wadadekar, Y., Kembhavi, A.K., Vijayagovindan, G.V 2010, MNRAS **409**, 1379

Voges, W. et al. 1999, A&A **349**, 389

Wang, Jian-Min, Chen, Yan-Mei, Luis, C.Ho& Ross, J.M. 2006, ApJ **642**, L111-L114

Wilson, A.S. & Colbert, E.J.M. 1995, ApJ **438**, 62

Wright, E.L.,Eisenhardt, Peter R.M.,Mainzer, A.K., et al. 2010, AJ **140**, 1868

Table 1: **The results of two dimensional bulge-disk decomposition**. Here m_b, m_d are the magnitudes of bulge and disk components and m_{tot} is the total magnitude. CFHT_x and SDSS_x denote the fits using either CFHT or the SDSS images in filter band x. All magnitudes are k-corrected and also corrected for galactic extinction, as described in the main text.

Telescope (filter)	m_b (mag)	m_d (mag)	m_{tot} (mag)
CFHT_g	17.14 ± 0.01	15.18 ± 0.01	15.02 ± 0.01
CFHT_r	16.36 ± 0.01	14.75 ± 0.01	14.53 ± 0.01
SDSS_g	17.52 ± 0.03	15.15 ± 0.01	15.03 ± 0.03
SDSS_r	16.56 ± 0.02	14.72 ± 0.01	14.54 ± 0.02
SDSS_i	16.22 ± 0.02	14.43 ± 0.01	14.24 ± 0.02
SDSS_z	15.72 ± 0.04	14.34 ± 0.01	14.07 ± 0.04

Table 2: **The results of two dimensional bulge-disk decomposition**. Here n is the Sérsic index, r_e, r_d are the bulge and disk scale lengths, and b/a_b, b/a_d are the axis ratios (semi minor/semi major) of the bulge and disk components respectively. CFHT_x and SDSS_x denote the fits using either CFHT or the SDSS images in filter band x. The fitting procedure is described in the main text.

Telescope (filter)	r_e (kpc)	n	r_d (kpc)	b/a_b	b/a_d
CFHT_g	1.18 ± 0.01	1.05 ± 0.02	7.51 ± 0.01	0.56 ± 0.01	0.53 ± 0.01
CFHT_r	1.25 ± 0.01	1.26 ± 0.02	7.06 ± 0.01	0.56 ± 0.01	0.53 ± 0.01
SDSS_g	0.87 ± 0.13	0.26 ± 0.58	5.64 ± 0.03	0.44 ± 0.08	0.54 ± 0.01
SDSS_r	1.02 ± 0.07	0.30 ± 0.26	5.38 ± 0.03	0.44 ± 0.04	0.55 ± 0.01
SDSS_i	1.12 ± 0.03	0.55 ± 0.15	5.18 ± 0.03	0.49 ± 0.03	0.56 ± 0.01
SDSS_z	1.09 ± 0.06	0.95 ± 0.26	5.10 ± 0.08	0.66 ± 0.04	0.54 ± 0.01

Table 3: ***WISE* mid-infrared magnitudes and luminosities for J2345-0449 .** Magnitudes with their errors are given in the first row in the four mid-IR bands. Second row shows the derived luminosities in erg s^{-1}. In third row the luminosity is shown in solar units and the fourth row shows the signal-to-noise ratios of detection in four bands.

WISE band (Wavelength)	W1 $3.4\,\mu$m	W2 $4.6\,\mu$m	W3 $12\,\mu$m	W4 $22\,\mu$m
Magnitude	11.882 ± 0.023	11.818 ± 0.023	9.001 ± 0.028	7.096 ± 0.100
Luminosity	6.71×10^{43}	2.88×10^{43}	2.62×10^{43}	2.26×10^{43}
Luminosity ($L_\odot$)	4.04×10^{11}	4.41×10^{11}	5.69×10^{12}	3.35×10^{13}
S/N ratio	47.9	47.8	38.7	10.9

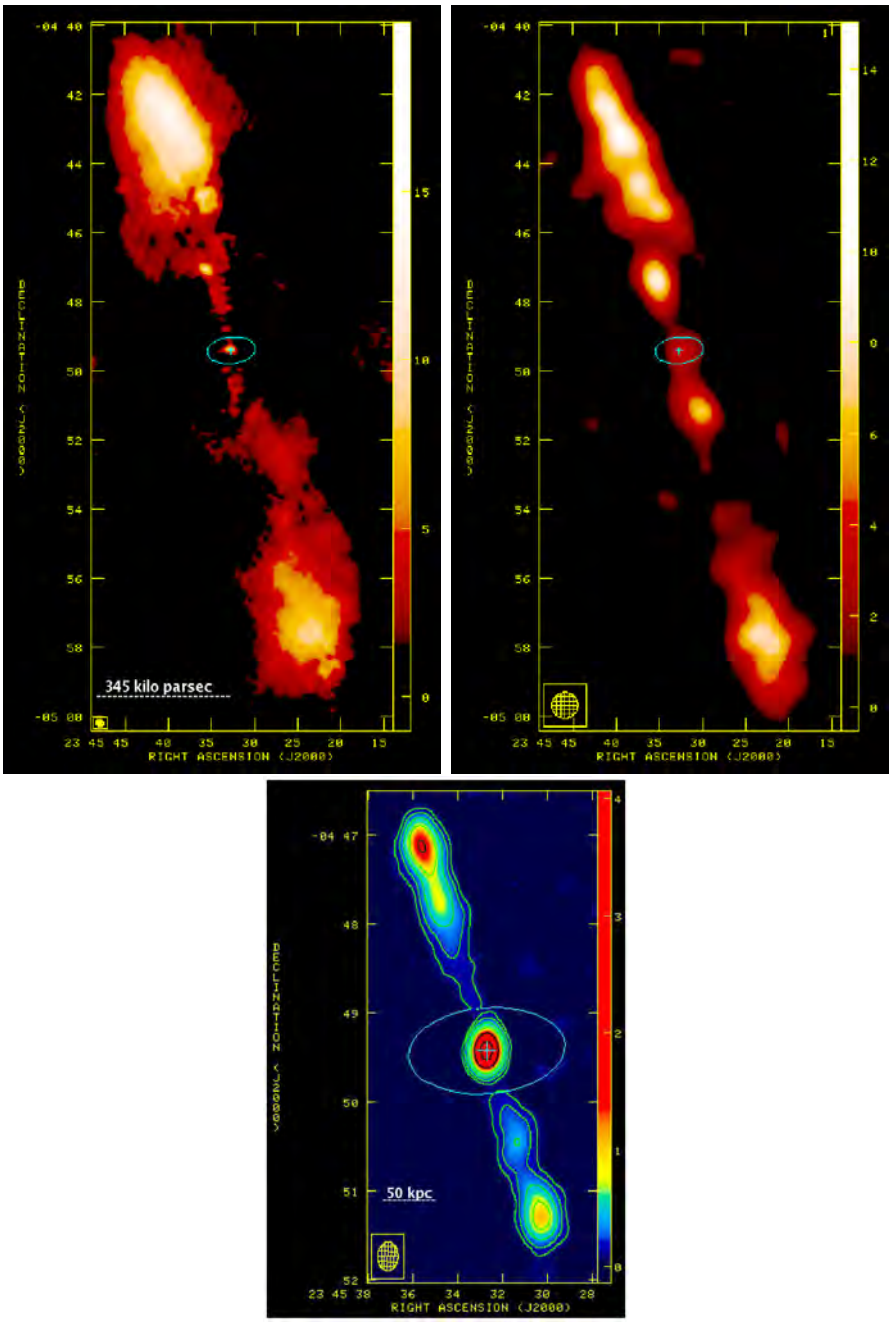

Fig. 1.— **The radio images of galaxy J2345-0449 .** (left) The 325 MHz image taken with GMRT (beam FWHM: $15.22'' \times 11.35''$ at 62.3°). (right) VLA 1.4 GHz image, taken from the NRAO VLA Sky Survey (NVSS), shown on the same scale (beam FWHM: $45'' \times 45''$). The diffuse emission near inner lobes is better visible at lower frequency, tracing the back-flowing steep-spectrum plasma of the outer lobes. An outline of the host spiral galaxy is drawn in blue, scaled to about thrice the optical disk size for clarity. (bottom) VLA 4.8 GHz image of the inner radio-double, showing the AGN core, bipolar radio-jets and the FR-II lobes (beam FWHM: $19.8'' \times 13.3''$ at 178.5°). Contour levels are: (-0.1, 0.1, 0.2, 0.4, 0.8, 1.6 and 3.2 mJy/beam). The spatial resolution (beam) is shown by a yellow ellipse within a box in each panel. The color wedges show the flux density levels in (mJy/beam). The bright, unresolved radio core at 4.8 GHz coincides within 0.15 arcsec with the nucleus of the spiral galaxy at right ascension: $23h\ 45m\ 32.71s$, declination: $-04°\ 49'\ 25.32''$ (J2000), thus firmly establishing it to be the optical host of the radio galaxy.

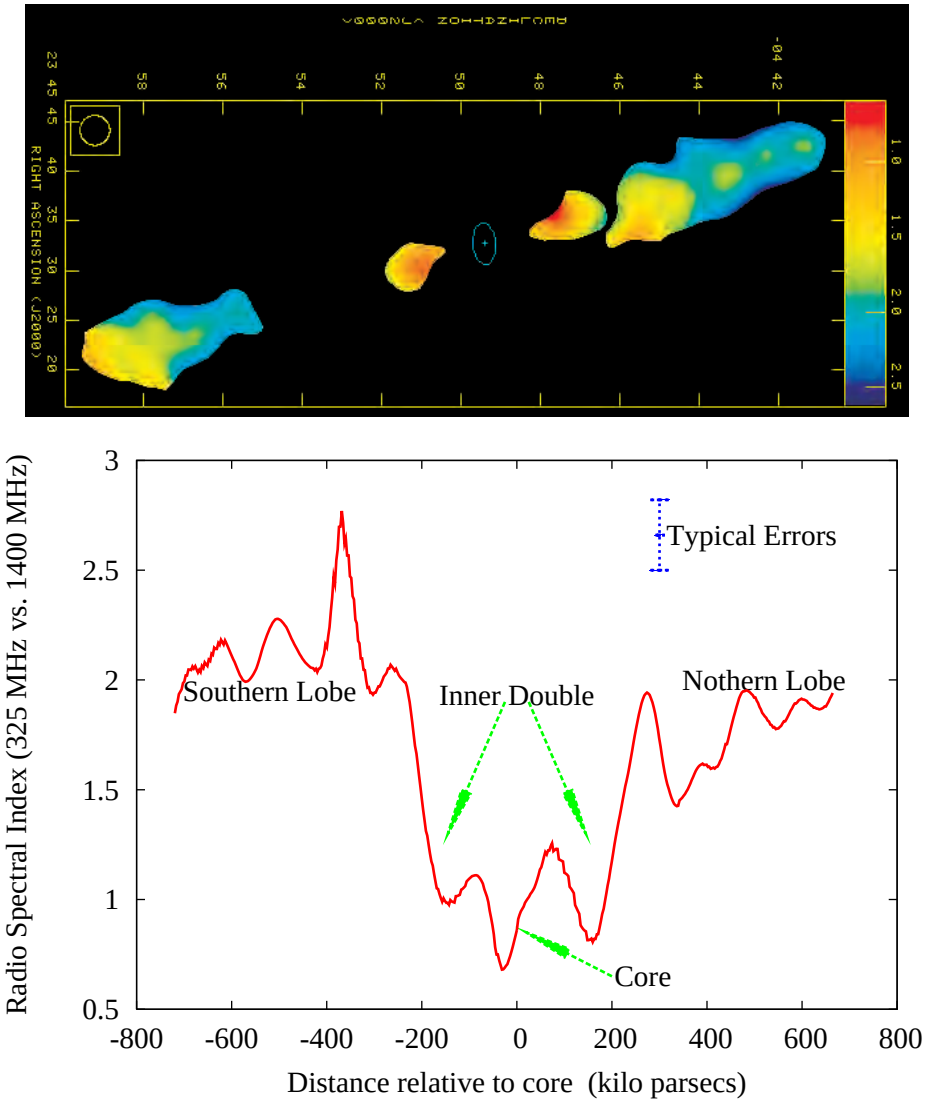

Fig. 2.— (Top) The spectral index image (rotated by 90 degrees), and (Bottom) the 1D spectral index profile, drawn along the brightness ridge of the source J2345-0449 between 325 MHz (GMRT) and 1400 MHz (VLA/NVSS) frequency is shown. In the spectral index map all pixels having flux density below 2 mJy/beam at 1400 MHz ($\sim 4\sigma$) and 15 mJy/beam at 325 MHz ($\sim 5\sigma$) have been blanked to prevent spurious structures from appearing in the map. An outline of the optical galaxy is shown by a blue ellipse, and the yellow circle within a box shows the $45'' \times 45''$ beam. The spectral index α is defined as: flux density (S_ν) $\propto$ frequency$(\nu)^{-\alpha}$. Typical error (1 σ) in the estimation of spectral index is shown at the top right corner of the 1D profile figure. The positions of radio core, the inner double lobes and the outer lobes of the radio source have been marked. Note a sharp increase in the spectral index between the inner and outer radio lobe pairs.

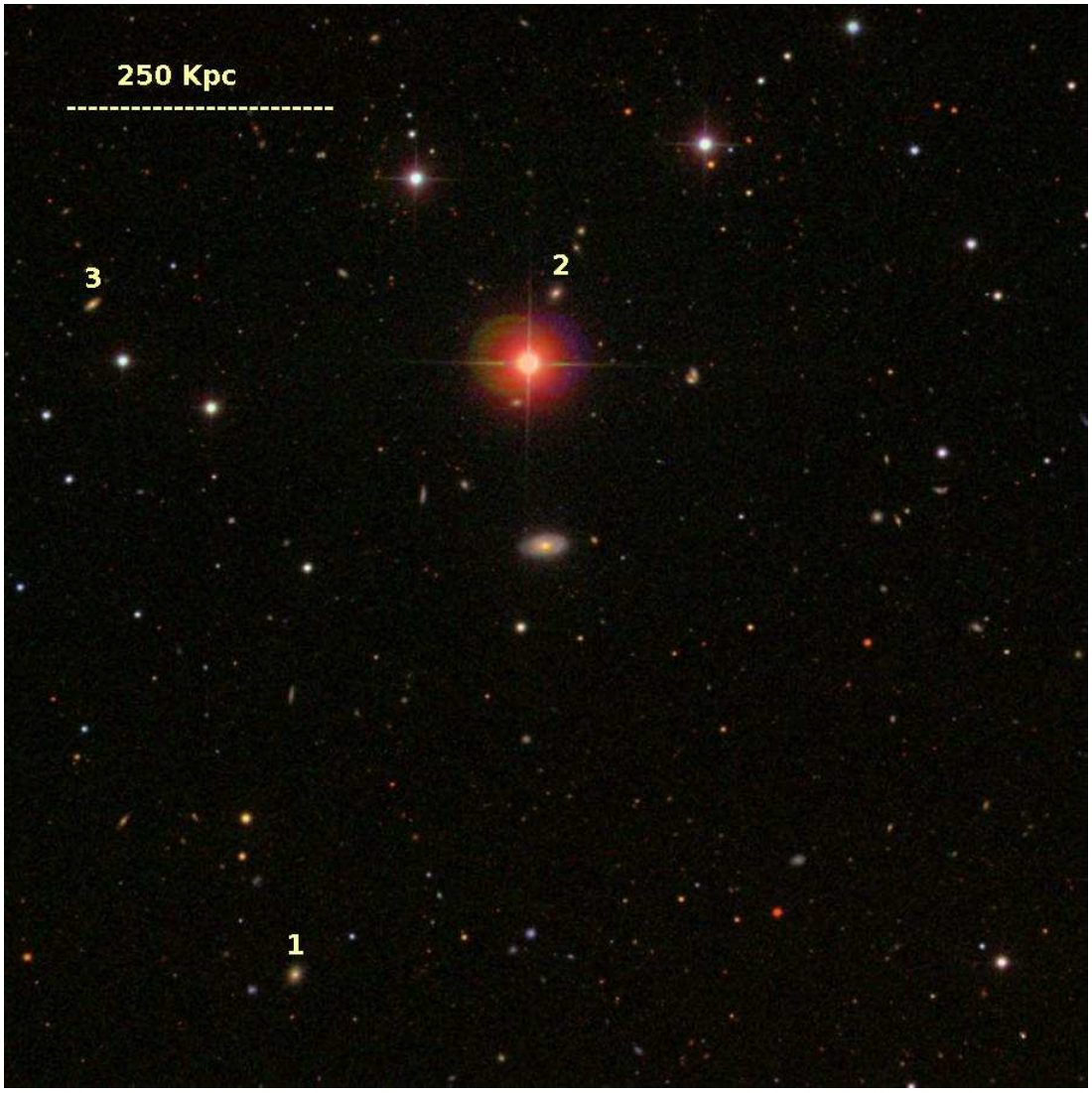

Fig. 3.— The large scale galactic environment around J2345-0449. The color image taken from the *Sloan Digital Sky Survey-III*, shows a field of view of $\sim 1\,\mathrm{Mpc} \times 1\,\mathrm{Mpc}$ centered on J2345-0449. The three nearest and brightest galaxies are marked in the descending order of their brightness in r-band; galaxy no. 1 ($m_r = 16.50$, $z_{\rm ph} = 0.0697$), galaxy no. 2 ($m_r = 16.87$, $z_{\rm ph} = 0.0615$) and galaxy no. 3 ($m_r = 17.07$, $z_{\rm ph} = 0.0798$). Here $z_{\rm ph}$ denotes the photometric redshift obtained from SDSS. The magnitude of spiral galaxy J2345-0449 is $m_r = 14.40$ in r with spectroscopic redshift 0.07556. All magnitudes are galactic extinction corrected and taken from SDSS.

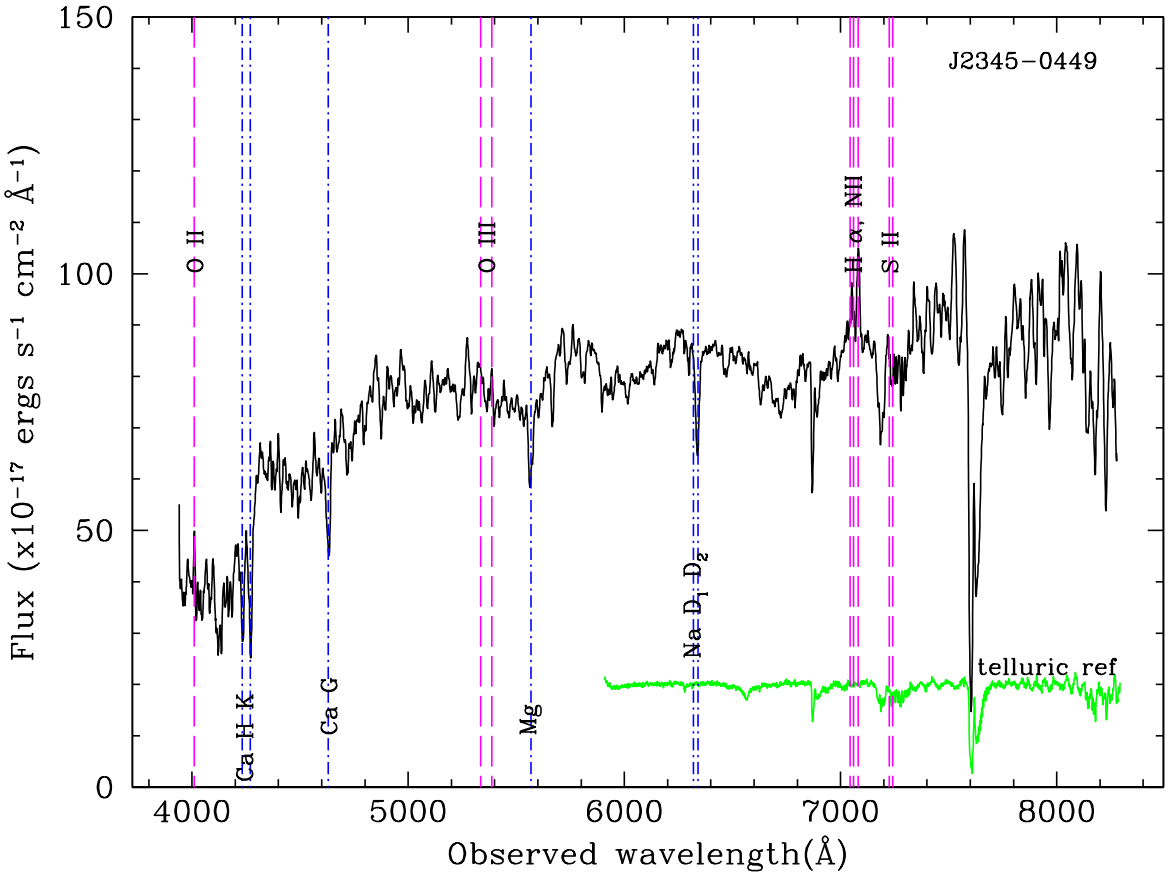

Fig. 4.— Major axis spectrum taken with IFOSC on IUCAA 2m telescope, centered on the nucleus. The absorption lines are marked by blue dot-dashed lines and the expected positions of the emission lines are marked with magenta color dashed lines. The red edge of the spectrum is contaminated by Telluric features. A Telluric reference spectrum is shown in green color at the bottom.

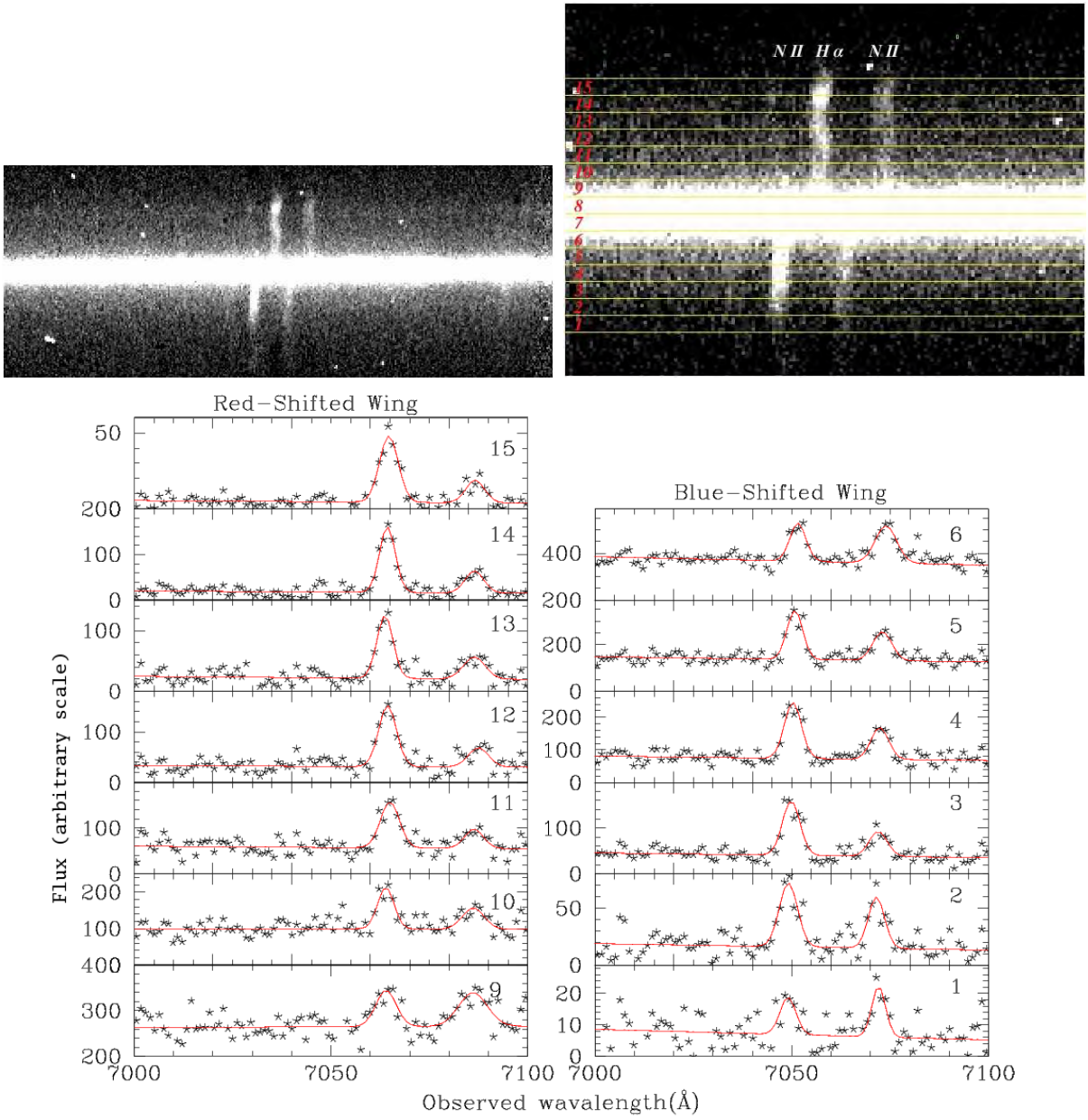

Fig. 5.— Upper panels: 2-D images showing the long-slit spectrum near the Hα and [NII] emission lines of galaxy J2345-0449 . Locations of different sub-apertures (numbers 1 to 15) used to derive the rotation curve of galaxy are marked in the zoomed right hand side image. Wavelength direction is horizontal, increasing to the right and the spatial direction is vertical. A sharply rising flat rotation curve is clearly evident in the shape of both Hα and [NII] lines marked here. Lower panels: 1-D spectra extracted at different sub-apertures as indicated in the above figure. Gaussian fits to Hα and [NII] lines are shown for the blue and red shifted wings of the spectra. The flux scale is arbitrary. No significant Hα emission was detected in the central apertures numbered 7 and 8. The parameters derived from the Gaussian fits are used to obtain the rotation curve (Figure 6), and the radial dependence of star formation rate and metallicity (Figure 7).

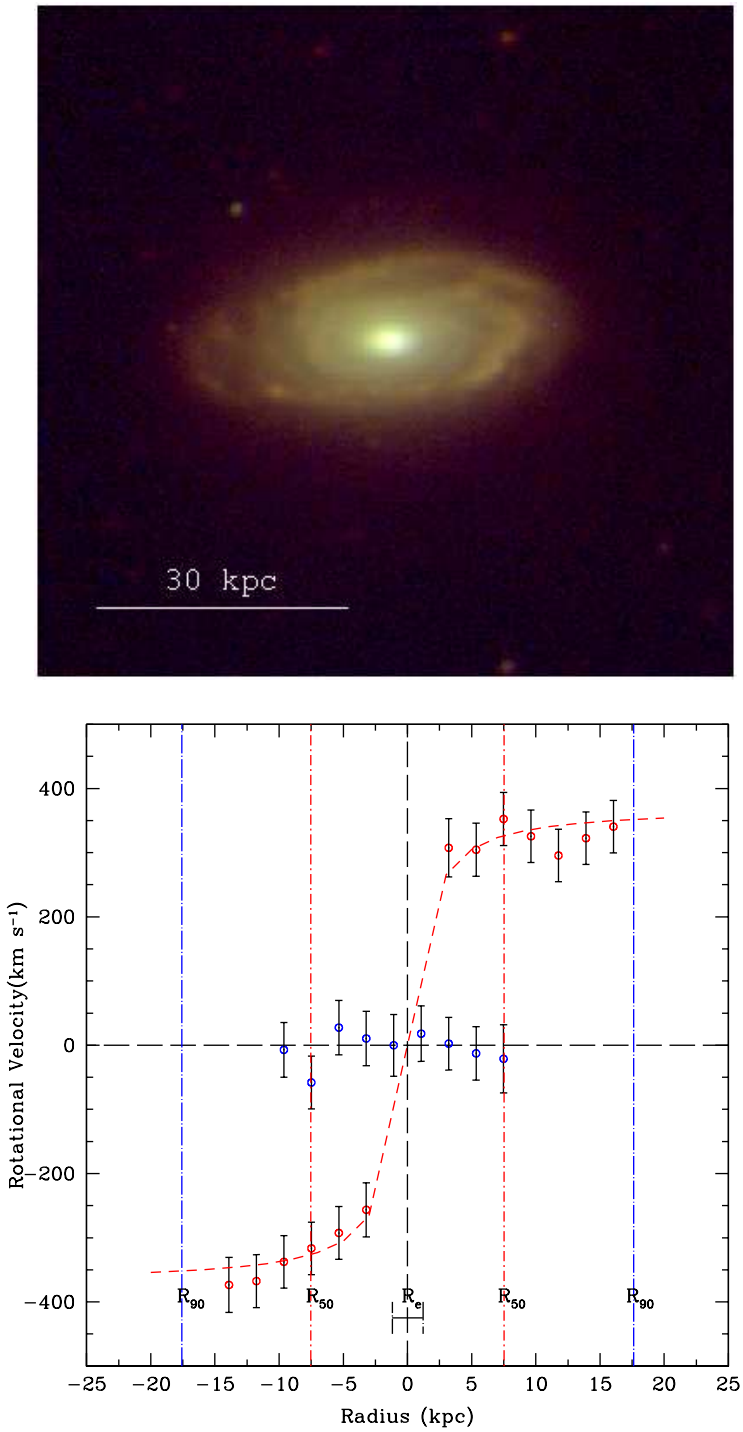

Fig. 6.— **The optical image and the rotation curve of spiral galaxy J2345-0449.** (top) A color composite from combining the deep optical images taken with the *MegaCam* on Canada-France-Hawaii Telescope (CFHT) in sub-arcsecond seeing. (bottom) shows the rotation curve of galaxy (red dashed curve) derived from the kinematics of Balmer Hα line in the long-slit spectrum taken along the major-axis (red data points) and minor-axis (blue data points). The rotational velocity is shown without the sin(i) correction for inclination. The major axis data shows a clear rotation signature while no such rotation is evident across the minor axis, clear evidence that the emission originates in a tilted rotating disk. For reference the scale length of stellar bulge component ($R_{\rm e}$) and the radii containing 50% (R_{50}) and 90% (R_{90}) of total optical light in the r-band is shown by red and blue dot-dashed vertical lines.

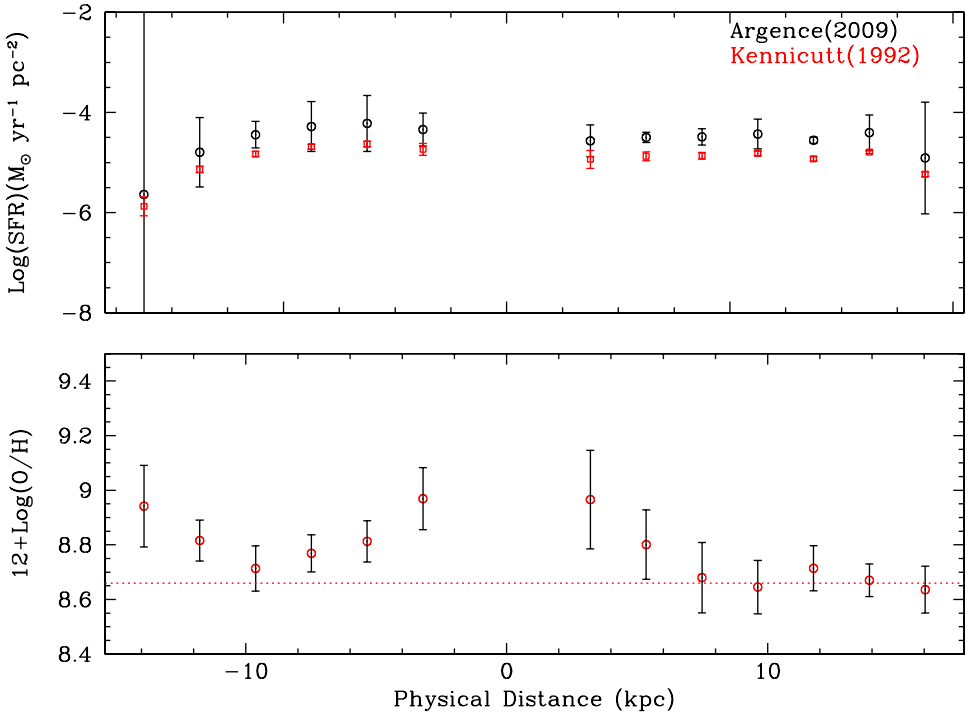

Fig. 7.— The surface star formation rate (SFR) computed at different radial positions along the major axis of the galaxy is shown in the top panel. The circles and squares are the values computed using the prescription given by Argence & Lamareille (Argence & Lamareille 2009) and Kennicutt (Kennicut 1992) respectively. Here we have not applied any correction for dust extinction. The derived Oxygen abundances are shown in the lower panel. The red horizontal dashed line marks the solar Oxygen abundance.

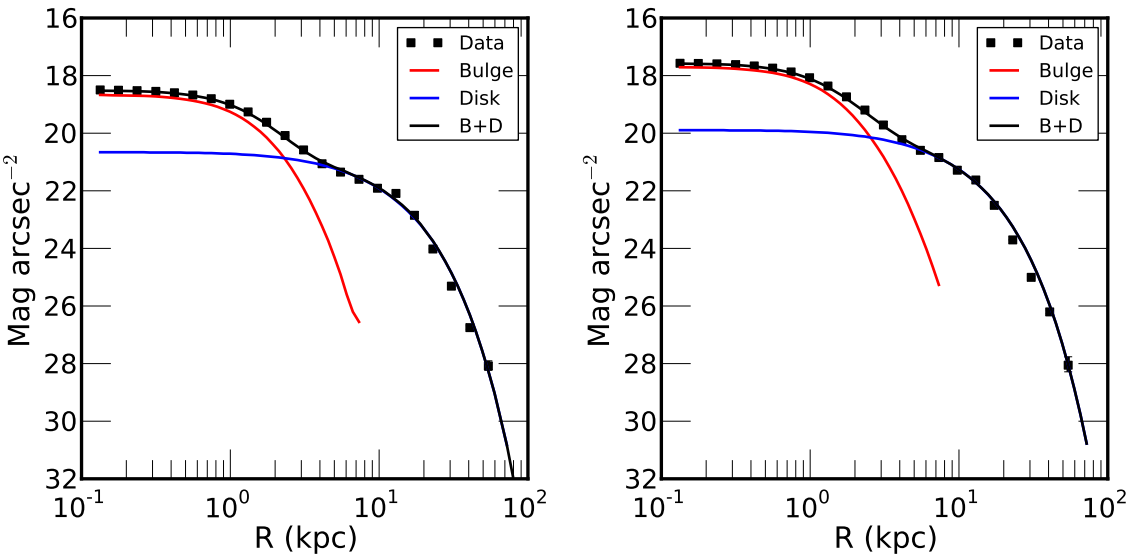

Fig. 8.— One dimensional surface brightness profile comparison. The black squares are observational data points obtained from CFHT image in g-band (left panel) and in r-band (right-panel). Red and blue lines are the model profiles for the bulge and disk components respectively. The black line shows the combined profile by adding the bulge and disk parts. The model profiles were obtained from a point spread function (PSF) convolved image generated by the GALFIT software, as described in the main text.

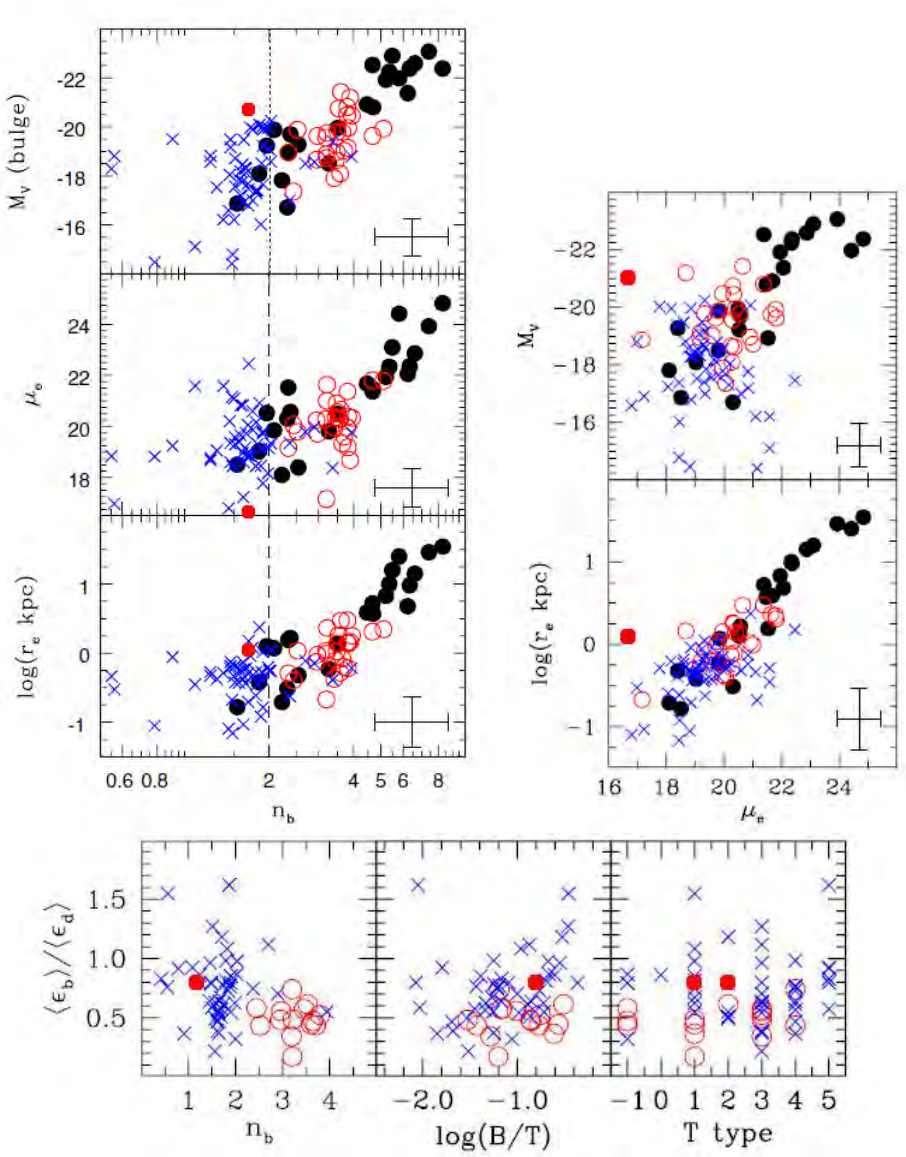

Fig. 9.— These figure panels show the comparison of structural and photometric properties of the bulge in present spiral galaxy J2345-0449 with bulges in other galaxies (both classical and pseudo bulges) as shown in (Fisher & Drory 2008). Here n_b, M_V, r_e and μ_e denote the Sérsic index, absolute V magnitude, scale radius and average surface brightness within r_e of bulge respectively. The dashed line in the first figure panel separates the classical bulges ($n_b > 2$) from pseudo bulges ($n_b < 2$). ϵ_b and ϵ_d are the ellipticity of bulge and disk components, and B/T is bulge to total light ratio. T-type is the morphological type of the galaxy (see main text). Blue crosses and red open circles represent the pseudo-bulges and classical bulges respectively in spirals, the filled red dot represents the present galaxy J2345-0449, while black filled points correspond to the ellipticals. J2345-0449 clearly belongs to the pseudo bulge category as seen on most of these plots. **We show two red dots in last figure panel; one for T-type = 1 (Sa) and other for T-type = 2 (Sab). This is to take care of the uncertainty in the visual T-type of the present galaxy**.